

## High-resolution $n = 3$ to $n = 2$ spectra of neonlike silver

P. Beiersdorfer, M. Bitter, S. von Goeler, S. Cohen, K. W. Hill, and J. Timberlake  
*Plasma Physics Laboratory, Princeton University, Princeton, New Jersey 08544*

R. S. Walling, M. H. Chen, P. L. Hagelstein, and J. H. Scofield  
*Lawrence Livermore National Laboratory, Livermore, California 94550*

(Received 6 March 1986)

Spectra of the  $n = 3$  to  $n = 2$  transitions in neonlike silver emitted from the Princeton Large Torus have been recorded with a high-resolution Bragg-crystal spectrometer. The measurements cover the wavelength region 3.3–4.1 Å and include the forbidden  $3p \rightarrow 2p$  electric quadrupole lines. Transitions in the adjacent sodiumlike, magnesiumlike, and aluminumlike charge states of silver have also been observed and identified. The Ly- $\alpha$  spectra of hydrogenlike argon and iron, the  $K\alpha$  spectra of heliumlike argon, potassium, manganese, and iron, and the  $K\beta$  spectrum of heliumlike argon fall in the same wavelength region in first or second order and have been measured concurrently. These spectra provide a coherent set of wavelength reference data obtained with the same spectrometer and from the same tokamak. This set is used as a basis to compare wavelength predictions for one- and two-electron systems to each other and to determine the transition energies of the silver lines with great accuracy.

### I. INTRODUCTION

Because of its closed-shell configuration, the neonlike charge state is relatively stable, and consequently is the dominant charge state over a wide range of plasma parameters. As a result, neonlike ions of medium and high  $Z$  are present in a variety of high-temperature plasma sources. Strong line radiation involving the  $n = 3$  to  $n = 2$  transitions in neonlike ions has been observed from tokamaks,<sup>1–4</sup> laser-produced plasmas,<sup>5–8</sup> gas-puff  $z$  pinches,<sup>9</sup> exploding wires,<sup>10</sup> vacuum sparks,<sup>11</sup> and the solar atmosphere.<sup>12–15</sup>

The properties of neonlike ions suggest their use for diagnostic purposes. In tokamaks, for example, neonlike ions are employed to study transport and confinement of high- $Z$  impurity ions.<sup>16–18</sup> Spectra from neonlike systems may also provide diagnostic information<sup>19–21</sup> on plasma electron temperature, electron density, charge-state abundances, or ion temperatures, similar to the diagnostic applications of heliumlike systems.<sup>22,23</sup>

Recent experiments have demonstrated amplification and lasing in the soft-x-ray region based on an electron-collisional excitation scheme involving neonlike ions.<sup>24,25</sup> A population inversion was achieved between the  $2p^{53p}$  and  $2p^{53s}$  levels in neonlike selenium ( $Z = 34$ ) by making use of the fact that the radiative decay rates to the  $2p^6$  ground state are vastly different for the two levels due to the dipole-selection rules. Subsequent experiments using yttrium ( $Z = 39$ ) and molybdenum ( $Z = 42$ ) have extended this scheme to elements of higher  $Z$  and obtained lasing at shorter wavelengths. For an understanding of these experiments, accurate determinations of the energy levels and the excitation mechanisms are important.

In this paper we present high-resolution spectra of the  $n = 3$  to  $n = 2$  transitions in neonlike silver ( $Z = 47$ ) from tokamak discharges in the Princeton Large Torus (PLT).

The PLT plasmas have electron densities around  $3 \times 10^{13} \text{ cm}^{-3}$  and electron temperatures around 3 keV. At these densities collisions are unimportant in depopulating the excited states of the silver ions. Consequently, the spectra are measured in a weak-collisional limit. The observations include six allowed electric dipole ( $E1$ ) transitions between the  $(2s2p^63p)_{J=1}$ ,  $(2s^22p^53s)_{J=1}$ , and  $(2s^22p^53d)_{J=1}$  upper states and the  $(2s^22p^6)_{J=0}$  ground state and the three forbidden electric quadrupole ( $E2$ ) transitions between the  $(2s^22p^53p)_{J=2}$  upper states and the ground state. We have used the observation of the latter transitions to obtain the intrashell energy-level differences of interest in soft-x-ray lasing schemes. The observation of  $E2$  transitions in neonlike systems has been reported for the first time only very recently from beam-foil experiments.<sup>26</sup> Our observations also include the magnetic quadrupole ( $M2$ ) transition between the  $(2p^5_{3/2}3s_{1/2})_{J=2}$  upper state and the ground state. Due to its small decay rate the  $M2$  transition cannot be observed in beam-foil experiments, nor can it be observed in high-density laser-produced or  $z$ -pinch plasmas because of the collisional deexcitation of the  $(2p^5_{3/2}3s_{1/2})_{J=2}$  level. This line provides additional information on intrashell transitions, and has been of interest in astrophysics.<sup>12–15</sup> We have also observed satellite lines situated on the long-wavelength side of the neonlike  $E1$  transitions. These lines have been identified as  $n = 3$  to  $n = 2$  transitions in sodiumlike, magnesiumlike, and aluminumlike silver.

Silver represents the element with the highest  $Z$  which has been observed in its neonlike charge state in a tokamak. Previously, the highest- $Z$  element in the neonlike isoelectronic sequence observed in a tokamak was molybdenum ( $Z = 42$ ).<sup>4</sup> Apart from tokamak observations, x-ray spectra of elements in the neonlike isoelectronic sequence as high as xenon ( $Z = 54$ ) have been measured in laser-produced plasmas<sup>8</sup> and from beam-foil in-

teractions.<sup>26</sup> X-ray spectra of neonlike silver have been reported first from an exploding-wire source<sup>10</sup> and, more recently, from a low-inductance vacuum spark.<sup>11</sup>

As wavelength references we have recorded the Lyman- $\alpha$  lines of hydrogenic argon, and the  $K\alpha$  and the  $K\beta$  lines of heliumlike argon. In addition, the spectra of heliumlike potassium, of heliumlike manganese, and of heliumlike and hydrogenlike iron have been observed in the wavelength range of interest, in either first or second order. These spectra are also presented. Together with the argon lines these measurements form a coherent set of atomic data which have been obtained with the same spectrometer and crystal and from the same tokamak. This set of data allows us to measure the silver lines with great accuracy. Accurate measurements are especially important for many-electron systems, such as those of neonlike or sodiumlike ions, because multielectron and quantum-electrodynamical effects can reduce the accuracy of the wavelength calculations considerably. The set of wavelength data also allows us to compare the theoretical predictions for one- and two-electron systems to each other using the experimental results as a basis, and a small disparity between wavelength predictions from one- and two-electron calculations has been observed.

## II. EXPERIMENTAL ARRANGEMENT

The observed spectra are recorded from PLT plasma discharges with a Johann-type crystal spectrometer shown in Fig. 1. This spectrometer provides very high spectral resolution and is used to measure the plasma ion temperature via Doppler broadening of the resonance line of heliumlike iron.<sup>27</sup> A detailed description of the basic properties of the spectrometer is given in Ref. 28.

For the present experiment the spectrometer has been modified in order to access the wavelength region between 3.3500 and 4.1000 Å. The spectrometer uses a  $6 \times 1.5$

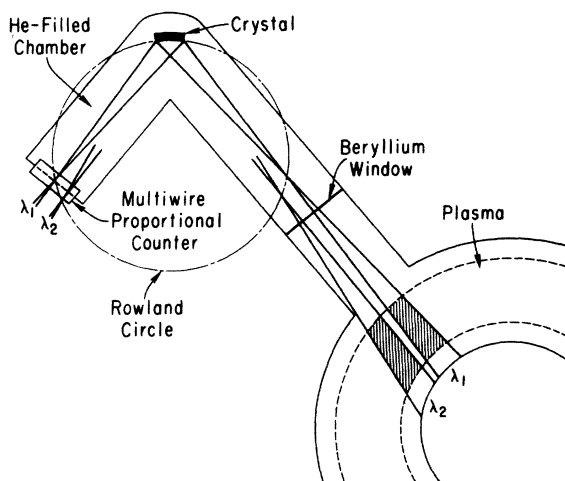


FIG. 1. Schematic of the high-resolution spectrometer on PLT. The spectrometer is viewing the horizontal midplane of PLT. In accordance with Bragg's law, x rays of different wavelength  $\lambda$  are focused at different positions along the position-sensitive detector.

$\times 0.03$ -in.<sup>3</sup> quartz crystal which has been bent to a radius of curvature of 276 cm. The crystal is cut parallel to the (11 $\bar{2}$ 0) plane. The  $2d_{\infty}$  spacing of this crystal plane is equal to the lattice constant  $a_0 = 4.913$  Å at 25°C.<sup>29</sup> A multiwire proportional counter with a sensitive area of  $10 \times 18$  cm<sup>2</sup> is employed to record the spectra. The counter is filled with a mixture of 90% krypton and 10% carbon dioxide. This gas mixture results in a constant detection efficiency over the observed range of photon energies. Adjustable lead apertures are placed in front of the crystal in order to limit the count rate to  $< 5 \times 10^5$  photons/sec. In our experiment, the illuminated length of the crystal was varied between 4 and 9 cm depending on discharge conditions.

The resolving power  $\lambda/\Delta\lambda$  of the spectrometer is about 3000 at  $\lambda = 4.0$  Å. This value is comparable to the values corresponding to the Doppler-broadened linewidth which are  $\lambda/\Delta\lambda \approx 3000$  for argon and  $\lambda/\Delta\lambda \approx 5000$  for silver at a typical ion temperature of 1 keV. Thus the resolution in our setup is approximately five times poorer than the resolution during the operation as an ion-temperature diagnostic.<sup>27</sup> This is due to the fact that in the present case the Bragg angle is 50° (instead of 65°) and the radius of curvature of the crystal is 276 cm (instead of 333 cm). The reduction in the resolution to a value comparable to that of the Doppler linewidth is a necessary compromise in order to adjust to the large dispersion range required for the recording of neonlike spectra. The wavelength interval which can be observed with one setting of the spectrometer is approximately 0.20 Å wide and is limited by the size of the viewing port on the PLT. In order to record the full wavelength range of interest between 3.3 and 4.1 Å, a minimum number of four alignments of the spectrometer is necessary. In the present experiment, the spectrometer was realigned to different Bragg angles a total of eight times. This allows us to record spectra which partially overlap. Since the alignment of the spectrometer could be changed only between PLT run days, the different settings of the spectrometer correspond to discharges from different days. The experimental conditions are thus not exactly the same for all of the silver spectra observed. As a result, the intensities ratios of silver lines recorded in different settings are not very reliable.

## III. HYDROGENLIKE AND HELIUMLIKE SPECTRA

Hydrogenic and heliumlike ions are the simplest atomic systems, and their wavelengths are theoretically known to a high degree of accuracy. The resonance lines of these ions are therefore well suited as references for measuring the wavelengths of lines emitted from more complex systems.

In the wavelength region investigated we have observed several hydrogenlike and heliumlike spectra. These include the Ly- $\alpha$  spectra of argon and iron, and the  $K\alpha$  spectra of heliumlike argon, potassium, manganese, and

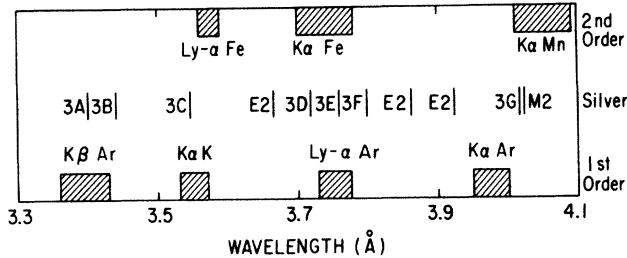


FIG. 2. Overview of the spectra observed in the wavelength range 3.30–4.10 Å in first order, and 1.65–2.05 Å in second order. The location of the neonlike  $n=3$  to  $n=2$  transitions of silver is shown relative to the hydrogenlike and heliumlike spectra. The notation used is that of Table III.

iron. We have also observed the  $K\beta$  spectrum of heliumlike argon. A schematic overview of the location of these spectra in the spectral range investigated is shown in Fig. 2. Note that the spectra of manganese and iron have been obtained in second-order Bragg reflection. The various spectra are shown in Figs. 3–7. Here we use the labels  $w$ ,  $x$ ,  $y$ , and  $z$  introduced by Gabriel<sup>30</sup> to denote the transitions  $1s2p\ ^1P_1$ ,  $1s2p\ ^3P_2$ ,  $1s2p\ ^3P_1$ , and  $1s2s\ ^3S_1$  to the  $1s^2\ ^1S_0$  ground state, respectively.

The spectra of iron, manganese, and potassium were ob-

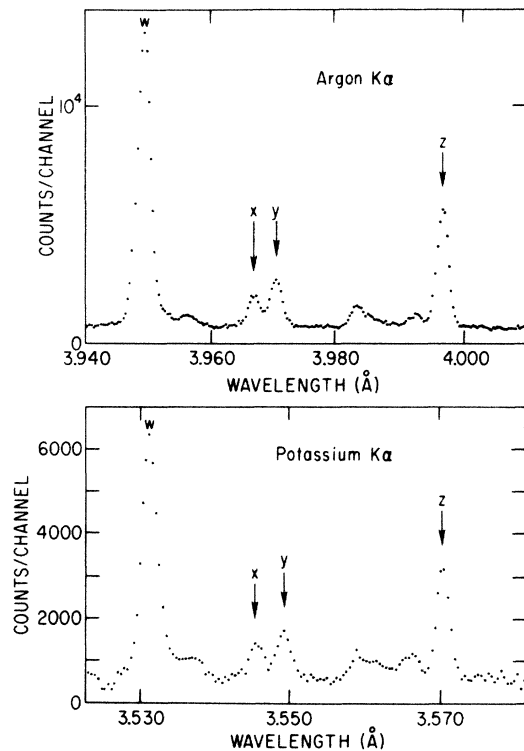


FIG. 3.  $K\alpha$  spectra of argon,  $Z=18$ , and potassium,  $Z=19$ . The lines are labeled according to the nomenclature of Ref. 30. Only the dominant transitions—the resonance line  $w$ , the intercombination lines  $x$  and  $y$ , and the forbidden line  $z$ —are labeled. The smaller peaks represent mainly dielectronic satellites.

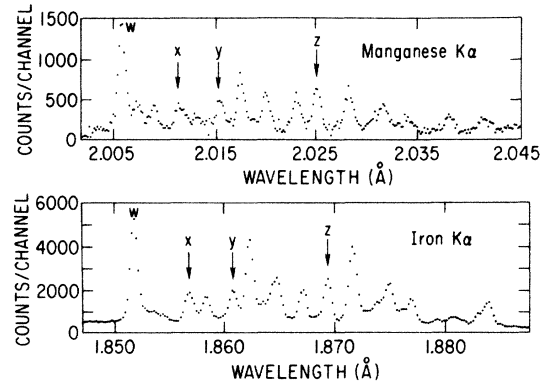


FIG. 4.  $K\alpha$  spectra of manganese,  $Z=25$ , and iron,  $Z=26$ , measured in second order. The dielectronic satellites are now very prominent.

served without deliberately introducing these elements into the plasma for spectroscopic purposes. Iron is indigenous to PLT tokamak plasmas, and its presence results from sputtering of the stainless-steel vacuum vessel. The presence of potassium and manganese in the plasma was unexpected. The origin of the manganese could be traced to the solder used in the connection between the ceramic break and the vacuum vessel. The origin of the potassium, however, remains unknown. The argon was deliberately introduced into the plasma in order to obtain additional wavelength references in the form of the argon Ly- $\alpha$  and the heliumlike  $K\alpha$  and  $K\beta$  resonance lines.

Experimental and theoretical wavelengths for the observed heliumlike lines are given in Table I. The observed Ly- $\alpha$  lines are listed in Table II. The measured wavelengths are rounded to the nearest multiple of  $5 \times 10^{-5}$  Å.

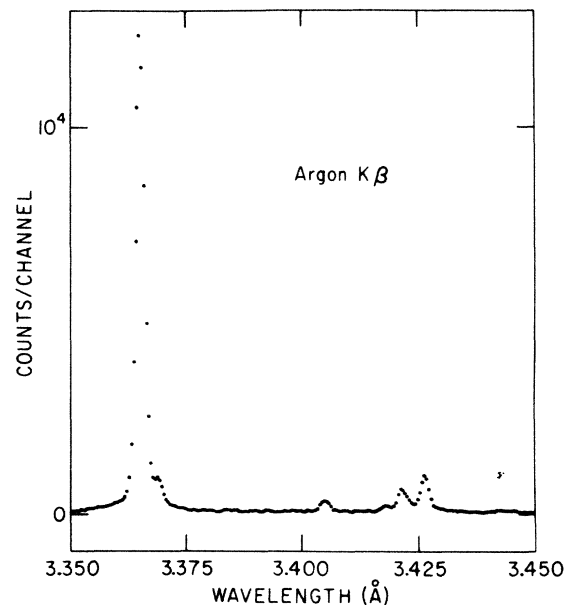


FIG. 5.  $K\beta$  spectrum of argon. The weaker, unmarked lines are satellite lines.

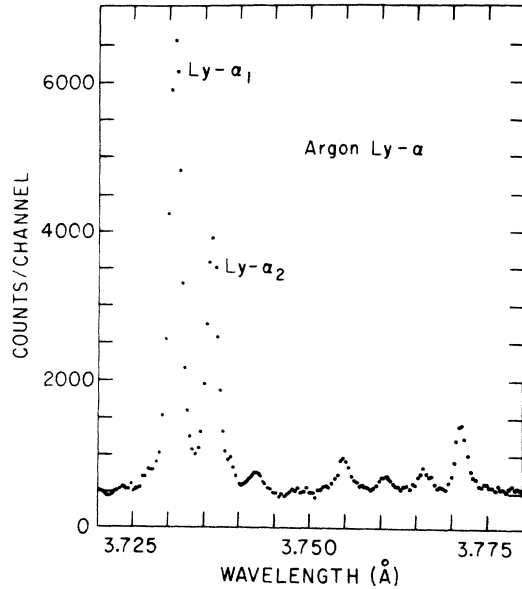


FIG. 6. Ly- $\alpha$  spectrum of argon. The weaker, unmarked lines are dielectronic satellites.

The theoretical values were taken from Vainshtein and Safronova<sup>31</sup> (heliumlike lines) and Mohr<sup>32</sup> (hydrogenlike lines). The lines with wavelength  $n\lambda \geq 3.900$  Å, where  $n$  is the order of diffraction in which the line is observed, are normalized to the theoretical value of 3.939 21 Å of the line  $w$  of heliumlike argon as calculated by Vainshtein and Safronova. For lines with wavelength  $n\lambda \leq 3.900$  Å we use the line  $w$  of heliumlike iron as a reference. Its

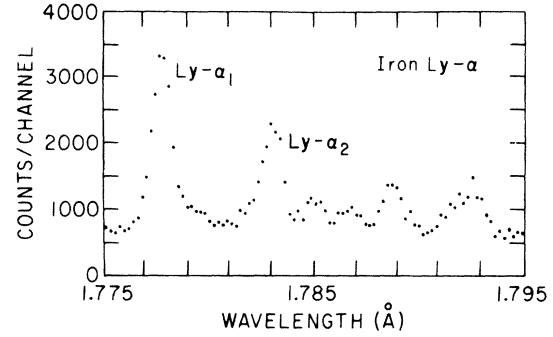


FIG. 7. Ly- $\alpha$  spectrum of iron. This spectrum represents a rare incidence on PLT. Hydrogenlike iron occurs only in very hot discharges. In this case the electron temperature exceeded 4 keV during lower hybrid heating.

value is set to  $\lambda = 1.85048$  Å, as also calculated by Vainshtein and Safronova. Two lines of reference are necessary for our measurement, because the separation between the line  $z$  of iron in second order and line  $w$  of argon is larger than the spectral range that can be observed with our spectrometer in one setting. Also, the region between the line  $z$  of iron and the line  $w$  of argon is devoid of other strong lines which could have served as a reference to interconnect the regions above and below 3.900 Å (see Fig. 2).

The wavelength  $n\lambda$  of a given line has been determined from Bragg's law<sup>33</sup>

$$n\lambda = 2d_{\infty} [1 - (2d_{\infty})^2 \delta / n^2 \lambda^2] \sin \theta, \quad (1)$$

TABLE I. Experimental and theoretical wavelengths of the resonance, intercombination, and forbidden lines of heliumlike argon, potassium, manganese, and iron. The theoretical values are from Ref. 31. The experimental values are rounded to the nearest multiple of  $5 \times 10^{-5}$  Å.

Element	Transition	Key	$\lambda_{\text{expt}}$ (Å)	$\lambda_{\text{theor}}$ (Å)
Argon <sup>a</sup>	$1s2p\ ^1P_1 \rightarrow 1s^2\ ^1S_0$	$w$	3.949 21	3.939 21
	$1s2p\ ^3P_2 \rightarrow 1s^2\ ^1S_0$	$x$	3.966 05	3.965 99
	$1s2p\ ^3P_1 \rightarrow 1s^2\ ^1S_0$	$y$	3.969 35	3.969 40
	$1s2s\ ^3S_1 \rightarrow 1s^2\ ^1S_0$	$z$	3.994 10 <sup>b</sup>	3.994 28
Potassium <sup>c</sup>	$1s2p\ ^1P_1 \rightarrow 1s^2\ ^1S_0$	$w$	3.531 95	3.531 98
	$1s2p\ ^3P_2 \rightarrow 1s^2\ ^1S_0$	$x$	3.545 95	3.546 07
	$1s2p\ ^3P_1 \rightarrow 1s^2\ ^1S_0$	$y$	3.549 50	3.549 64
	$1s2s\ ^3S_1 \rightarrow 1s^2\ ^1S_0$	$z$	3.570 40 <sup>b</sup>	3.570 84
Manganese <sup>a</sup>	$1s2p\ ^1P_1 \rightarrow 1s^2\ ^1S_0$	$w$	2.006 15	2.006 15
	$1s2p\ ^3P_2 \rightarrow 1s^2\ ^1S_0$	$x$	2.011 90	2.011 85
	$1s2p\ ^3P_1 \rightarrow 1s^2\ ^1S_0$	$y$	2.015 90	2.015 85
	$1s2s\ ^3S_1 \rightarrow 1s^2\ ^1S_0$	$z$	2.025 40	2.025 57
Iron <sup>c</sup>	$1s2p\ ^1P_1 \rightarrow 1s^2\ ^1S_0$	$w$	1.850 48	1.850 48
	$1s2p\ ^3P_2 \rightarrow 1s^2\ ^1S_0$	$x$	1.855 55	1.855 46
	$1s2p\ ^3P_1 \rightarrow 1s^2\ ^1S_0$	$y$	1.859 60	1.859 53
	$1s2s\ ^3S_1 \rightarrow 1s^2\ ^1S_0$	$z$	1.868 30	1.868 24
Argon <sup>c</sup>	$1s3p\ ^1P_1 \rightarrow 1s^2\ ^1S_0$	$K\beta$	3.365 80	3.365 71

<sup>a</sup>Experimental wavelengths are normalized to the theoretical value of 3.949 21 Å for the line  $w$  of argon.

<sup>b</sup>Line blended with satellite  $j$  ( $1s2p^2D_{5/2} \rightarrow 1s^22p^2P_{3/2}$ ).

<sup>c</sup>Experimental wavelengths are normalized to the theoretical value of 1.850 48 Å for the line  $w$  of iron.

TABLE II. Experimental and theoretical wavelengths of the resonance lines of hydrogenic argon and iron. The theoretical values are from Ref. 32. The experimental values are rounded to the nearest multiple of  $5 \times 10^{-5}$  Å and are normalized to the theoretical value of 1.85048 Å of the line  $w$  of iron.

Element	Transition	Key	$\lambda_{\text{expt}}$ (Å)	$\lambda_{\text{theor}}$ (Å)
Argon	$2P_{3/2} \rightarrow 1S_{1/2}$	Ly- $\alpha_1$	3.731 50	3.731 10
	$2P_{1/2} \rightarrow 1S_{1/2}$	Ly- $\alpha_2$	3.736 80	3.736 52
Iron	$2P_{3/2} \rightarrow 1S_{1/2}$	Ly- $\alpha_1$	1.778 20	1.778 02
	$2P_{1/2} \rightarrow 1S_{1/2}$	Ly- $\alpha_2$	1.783 60	1.783 44

where  $n$  is the order of diffraction,  $\theta$  is the Bragg angle, and  $\delta$  is the deviation of the index of refraction from unity. The value of  $\delta/\lambda^2$  is taken to be independent of wavelength and equal to  $3.64 \times 10^{-6}$  Å $^{-2}$  for quartz.<sup>34</sup>

The Bragg angle  $\theta$  of a line whose center position is observed in channel  $N$  is given by

$$\theta = \theta_c + \arctan[(N_c - N)\Delta x/D], \quad (2)$$

where  $\theta_c$  is the Bragg angle corresponding to the central channel number  $N_c$  of the detector.  $\Delta x$  is the distance between two adjacent channels, and  $D$  is the distance between crystal and detector. The arctangent is used because the detector is oriented perpendicular to the line connecting the crystal and the center of the detector, and not tangent to the Rowland circle (see Fig. 1).

The center position of a line is obtained from a least-squares fit of a single Voigt function to the experimental data. This Voigt fit is shown in Fig. 8 for the Ly- $\alpha_1$  line of argon. The ranges of data points used for the fit and the background determination are indicated in the figure. Due to the good counting statistics the statistical error for the center position of the line is only 0.015 channels (approximately 6  $\mu$ Å), as given by the least-squares analysis. Any line, however, may contain contributions from unresolved satellites produced by the dielectronic capture of an electron into an atomic level with quantum number  $n \geq 3$ .<sup>35-37</sup> These unresolved satellites occur mainly on the long-wavelength side and, in effect, increase the observed wavelength of the apparent resonance line. The magnitude of these satellites increases as  $Z^4$  and is temperature dependent. Hence, the presence of these satellites places an upper limit on the experimental certainty with which the wavelength of a given transition can be determined from a single-Voigt-function fit. A detailed description of this effect has been given in Ref. 23, where the wavelength shift of the apparent  $K\alpha$  line of heliumlike titanium was studied as a function of electron and ion temperatures and fitting limits. In this case, a wavelength shift of 0.1 mÅ was found at electron and ion temperatures of 1 keV.<sup>23</sup> Changing the fitting limits for the spectrum shown in Fig. 8 from a to b changes the value of the center position of the Ly- $\alpha_1$  line by 0.07 channels. In addition, the value of the center position has been found to vary between sets of data from different time intervals or

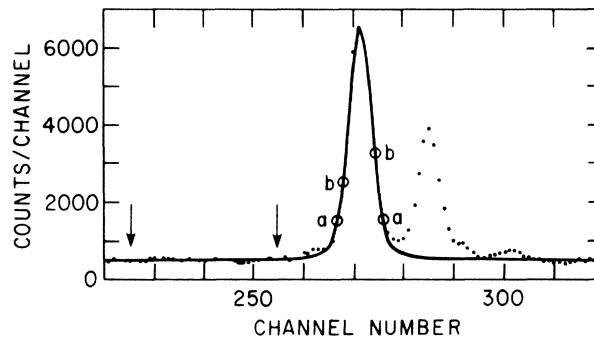


FIG. 8. Least-squares fit of a single Voigt function to the Ly- $\alpha_1$  line of argon. The arrows indicate the region used for the determination of the background. The pairs of points labeled a and b represent two different sets of fitting limits.

from different discharges—and thus different discharge conditions—by as much as 0.1 channel (40  $\mu$ Å). Error analyses for the center positions of the lines of the other elements listed in Tables I and II give similar results as the error analysis for the Ly- $\alpha_1$  line of argon. The uncertainties are slightly higher for those lines for which the counting statistics are not as good as those of the argon lines. For the weakest lines the uncertainty in determining the center positions is about  $1 \times 10^{-4}$  Å.

Once the channel number corresponding to the center position of a line is known, its wavelength is determined with respect to a reference line using Eqs. (1) and (2). Thus the experimental error of our wavelength measurements also depends on the value of  $\Delta x/D$ . Due to the finite thickness of the detector the value of  $D$  is slightly different for lines detected in first or second order. Photons detected in first order have lower energy and are absorbed by the detector gas sooner than photons detected in second order. The corresponding systematic difference in the effective distance  $D$  between first and second order is estimated to be 3 mm and has been taken into account. The absolute value of  $\Delta x/D$  is known to within  $2.5 \times 10^{-3}$ . The uncertainty of the measured wavelength separation between two nearby lines, say  $w$  and  $y$ , which results from the uncertainty in  $\Delta x/D$ , is about  $5 \times 10^{-5}$  Å, but it is larger for wavelengths which are further apart. The accuracy of the lines measured in second order is twice that of the lines measured in first order. The experimental wavelengths listed in Tables I and II have been rounded to multiples of  $5 \times 10^{-5}$  Å, i.e., the accuracy to which the center position of most lines is known. The experimental wavelengths obtained with different spectrometer settings have been reproducible to within 0.1 mÅ.

The measured wavelengths are found to be in good agreement with the theoretical values. Looking at the heliumlike lines we note that the agreement is almost perfect for the lines  $w$  and  $K\beta$ . The line farthest away from a reference line is the line  $K\beta$  of heliumlike argon. Despite this separation its experimental wavelength differs from the theoretical wavelength calculated by Vainshtein and Safronova<sup>31</sup> only by 0.1 mÅ. Good agreement between our measurements and the values given in

Ref. 31 is also found for the lines  $x$  and  $y$ , and the line  $z$  of the high- $Z$  elements, although some discrepancies can be noted. The largest discrepancy exists for the line  $z$  of heliumlike manganese. Here  $\Delta(n\lambda)$  is approximately 0.3 mÅ. The recent calculations by Vainshtein and Safronova<sup>31</sup> agree with our measurements of the relative spacings of the lines  $w$ ,  $x$ ,  $y$ , and  $z$  much more closely than earlier calculations by Safronova<sup>38</sup> where Lamb shifts had been neglected. We also would like to point out the fact that the determination of the wave length of the line  $z$  of argon and potassium is not very certain because the satellite  $j$  is blended with the line  $z$  for elements with  $Z < 20$ .

The measured values of the Ly- $\alpha$  lines of argon and iron, again using the theoretical value calculated by Vainshtein and Safronova for line  $w$  of iron as a reference, are found to be longer than the values predicted by Mohr.<sup>32</sup> The discrepancy  $\Delta(n\lambda)$  is approximately 0.4 mÅ for the lines of both elements and is larger than the estimate for our experimental uncertainty. Presuming that the wavelengths of the one-electron systems can be calculated with better accuracy than those of heliumlike ions, this discrepancy might indicate that the theoretical wavelengths predicted by Vainshtein and Safronova<sup>31</sup> for two-electron systems are somewhat too long. Absolute measurements of the wavelengths of the lines of hydrogenlike argon and iron and of heliumlike argon have been performed by Briand *et al.*<sup>39,40</sup> Unfortunately, the accuracy of these measurements of  $\pm 0.3$  mÅ is insufficient to resolve this question.

The data in Tables I and II represent a coherent set of wavelength data observed with the same spectrometer, the same crystal, and from the same tokamak, similar to a set of data from the TFR tokamak, at the Centre d'Etudes Nucléaires de Fontenay-aux-Roses, France, reported recently for heliumlike argon, scandium, vanadium, chromium, and manganese.<sup>41</sup> We have arbitrarily chosen the lines  $w$  of argon and iron as reference lines, and we have arbitrarily normalized our wavelength measurements to the theoretical values calculated in Ref. 31. However, one may equally well choose different heliumlike  $K\alpha$  or hydrogenlike Ly- $\alpha$  lines in our spectral range as reference for our experimental wavelengths. The close and consistent agreement found between our measurements and the theoretical predictions makes us confident that we can use these data to determine the wavelengths of the silver lines with similarly high accuracy. Since every silver line is close to a strong hydrogenlike or heliumlike reference line, as seen in Fig. 2, errors which are caused by uncertainties in the dispersion of the spectrometer can be minimized to  $\leq 0.15$  mÅ. The measurements of the silver lines will be discussed in the next section.

#### IV. SILVER SPECTRA

The silver was injected into the plasma via laser blow-off<sup>42</sup> during the quasi-steady-state phase of the discharge. The amounts of silver introduced were always kept at a level which did not cause a significant perturbation of the major plasma parameters such as electron temperature and density.<sup>43</sup> A minimum central electron temperature of approximately 2.4 keV was found to be necessary to observe silver in the neonlike charge state. For most of the

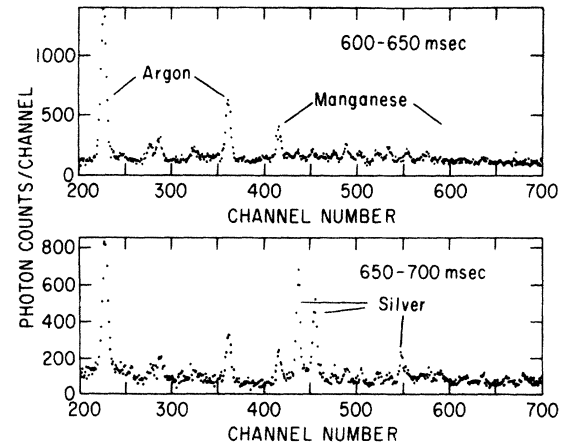


FIG. 9. Typical spectra recorded before and after injection of silver. The injection takes place at  $t=650$  msec. The x-ray flux in each case is integrated for 50 msec. The  $K\alpha$  spectra of heliumlike argon and manganese are clearly visible. The main silver lines appear at channels 435.7, 453.7, and 547.3. These lines correspond to the lines 3G, M2, and p in Fig. 13. The injection almost always causes a drop in the intensity of the radiation of other impurities. This effect is attributed to a replacement of indigenous plasma impurities by the newly injected one.

data obtained in Ohmically heated discharges the central electron temperature is in the range of 2.4–3.0 keV. Some data were obtained in lower-hybrid-heated discharges at somewhat higher electron temperatures. The central electron density varies between  $(1.5-5.0) \times 10^{13} \text{ cm}^{-3}$ . Peak line emission levels are attained about 40 msec after the silver injection. During this time the silver penetrates to the center of the plasma, while ionizing to the neonlike charge state. The line emission levels then drop as the silver exits the plasma diffusively and adheres to the limiter and the vacuum vessel. About 150–200 msec after the injection, depending on the amount of silver injected and the discharge conditions, the silver line emission decreases to a level at which the lines blend with the background from the bremsstrahlung and recombination continuum and cannot be observed anymore.

Typical spectra observed before and after laser blow-off injection are shown in Fig. 9. In the case shown, the laser was fired at 650 msec. Each of the two spectra is obtained by integrating the x-ray flux for a 50-msec time interval. In order to improve statistics we have added data from ten similar discharges together. The statistics can be improved further by adding two or three subsequent time groups, each of which is 50-msec long. The result of this is, of course, the same as integrating the x-ray flux over the 150–200-msec interval after injection. Usually, a comparison between the two spectra taken before and after injection readily identifies the silver lines. However, this is not always the case. In particular, silver lines which are located in the wavelength region dominated by the  $K\alpha$  spectrum of heliumlike iron cannot be identified as easily. This region is shown in detail in Fig. 10. In order to identify these lines we subtract a “background” iron spectrum from the spectrum containing the silver lines. As background spectra, one may use the spectra

recorded just before the silver injection. However, we have obtained best results by using spectra which have been recorded at the same time in the discharge and for similar plasma conditions but without silver injection. The intensities of the spectrum containing the silver lines and the background spectrum are normalized to each other before subtraction. For the case shown we have used the line  $z$  of heliumlike iron for normalization. The result of the subtraction is also shown in Fig. 10. The ratios of the various iron lines in a given spectrum may depend on a variety of factors such as the electron temperature and the presence of other impurities including silver. (Cf. Fig. 4 which shows an iron spectrum recorded from discharges with higher electron temperatures than the spectrum in Fig. 10.) Therefore, the exact appearance of the spectrum resulting from such a subtraction is sensitive to which line or set of lines is used to normalize the intensities of both spectra to each other. In some cases certain iron lines may be subtracted too much, and some lines too little, which may result in the appearance of "ghost" lines, the magnitude of which may be comparable to that of weak silver lines. Looking at Fig. 10 we note that the spectrum

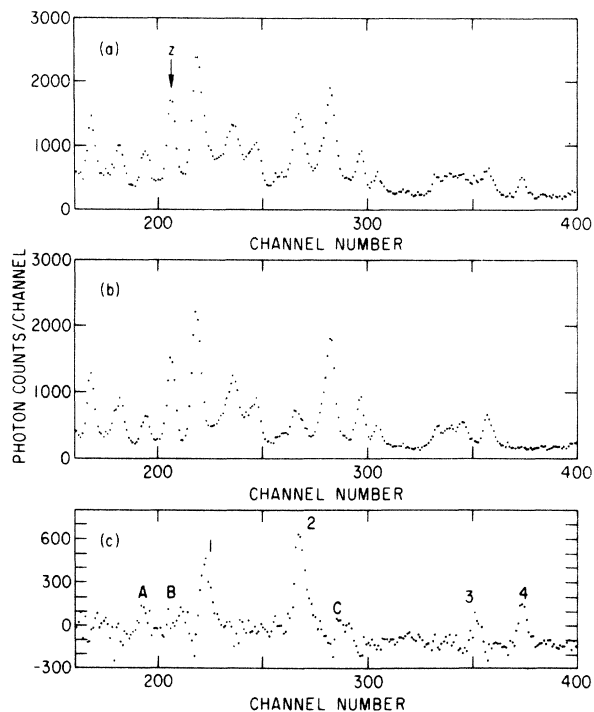


FIG. 10. Subtraction of the iron  $K\alpha$  "background" from a spectrum containing silver lines. In (a) the iron radiation in second order is mixed with the silver emission in first order. Here, the wavelength increases with channel numbers (cf. Fig. 4). In (b) the same wavelength region is shown but without silver lines. The discharge conditions for this spectrum are very similar to the conditions in (a) except that no injection took place. The spectrum (c) results from the subtraction of (a) minus (b). For this purpose the intensity of (b) is normalized to that of (a) using the line  $z$  of iron. Lines 1, 2, 3, and 4 have been identified as silver lines, i.e., lines  $l$ ,  $9$ ,  $\iota$ , and  $3F$ , respectively (cf. Fig. 13). Lines A, B, and C may be the result of over or under subtraction.

resulting from the subtraction reveals four well-resolved lines which are marked 1 through 4 in the figure. We also note a variety of smaller features, three of which are marked A, B, and C. In addition, we find that the subtraction has resulted in a general increase in the apparent noise level in the spectrum. We have repeated the subtraction using different lines for normalization, different background spectra, and different injection data. As a result, we are confident that the four lines 1–4 are silver lines (cf. Fig. 13). The nature of the other features remains uncertain, although we believe they are a result of the subtraction process, i.e., ghost lines.

In Figs. 11–14 we show the spectral range of the silver data obtained in the present experiment. The figures cover the wavelength region  $\lambda=3.36$ – $4.10$  Å. The spectra arising from other plasma impurities have been subtracted out in order to eliminate a confusing amount of spectral features in these figures. The region which contained the  $K\alpha$  spectrum of heliumlike iron has been hatched (Figs. 12 and 13). Since the subtraction increases the noise level, we have, for clarity, plotted all lines identified as silver lines with a Voigt function fit superimposed onto them. In Figs. 11–14, the experimental data are also compared to theoretical predictions for sodiumlike, magnesiumlike, and aluminumlike transitions. In the figures we have labeled the neonlike lines with upper-case letters. In particular, the  $E1$  transitions are labeled  $3A$ – $3G$ , according to the notation used in Ref. 44, and the electric and magnetic quadrupole transitions are labeled  $E2$  and  $M2$ , respectively. Sodiumlike lines are labeled with lower-case Roman letters. Magnesiumlike and aluminumlike lines are labeled with numbers and Greek letters, respectively. An asterisk or overbar is used to distinguish the several types of transitions we considered. We compared our measured line positions with wavelengths from *ab initio* calculations. This, in conjunction with a qualitative understand-

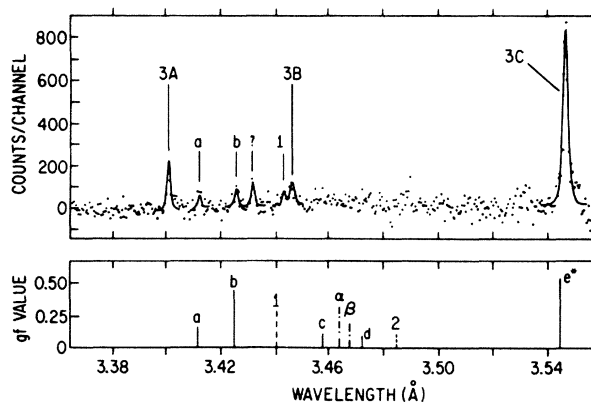


FIG. 11. Spectrum of silver in the wavelength region  $3.370$ – $3.550$  Å. This region includes the  $3p \rightarrow 2s$  transitions. The spectra of other impurities have been subtracted out for clarity. A theoretical spectrum containing sodiumlike, magnesiumlike, and aluminumlike transitions is shown below the experimental data. Neonlike transitions are labeled with upper-case letters; sodiumlike (solid), magnesiumlike (dashed), and aluminumlike (dot-dashed) lines are keyed with lower-case letters, with numbers, and with Greek letters, respectively.

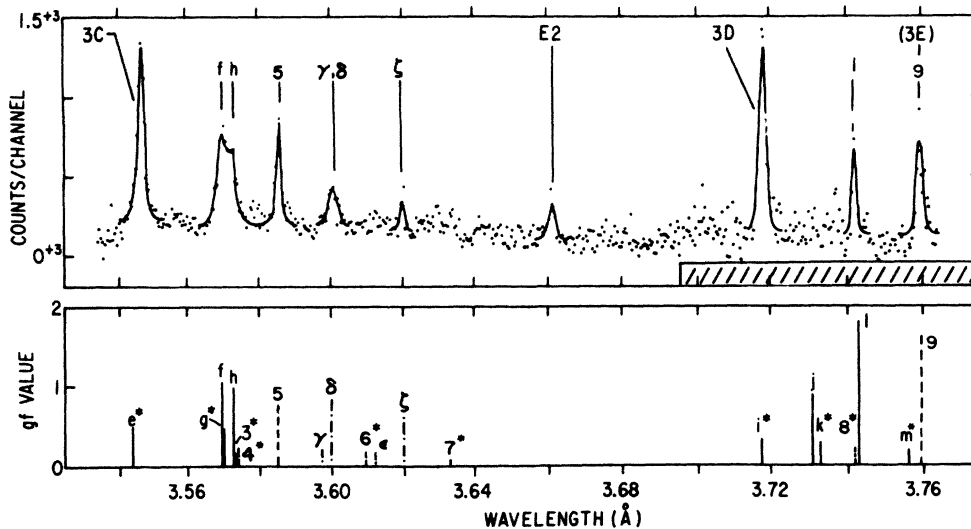


FIG. 12. Spectrum of silver in the wavelength region 3.540–3.760 Å. This region includes most of the  $3d \rightarrow 2p$  transitions. The spectra of other impurities have been subtracted out for clarity. The hatched region indicates the location of the  $K\alpha$  spectrum of heliumlike iron. A theoretical spectrum containing sodiumlike, magnesiumlike, and aluminumlike transitions is shown below the experimental data. Neonlike transitions are labeled with upper-case letters; sodiumlike (solid), magnesiumlike (dashed), and aluminumlike (dot-dashed) lines are keyed with lower-case letters, with numbers, and with Greek letters, respectively.

ing of the intensities, was the basis for our identifications. For all charge states  $\text{Ag}^{38+} - \text{Ag}^{34+}$  we have used wavelengths and oscillator strengths calculated from a relativistic atomic-structure code (RAC). This program calculates self-consistent Dirac-Fock orbitals from an average-configuration potential including exchange. For each charge state we included several configurations in the di-

agonalization for the eigenstates in order to get the wavelengths and oscillator strengths to good accuracy. The amount of configuration interaction included for the calculation of each charge state differed. In some cases we were not able to include all mixings between configurations in the same spectroscopic complex. The necessary computer memory and CPU time increases as the number

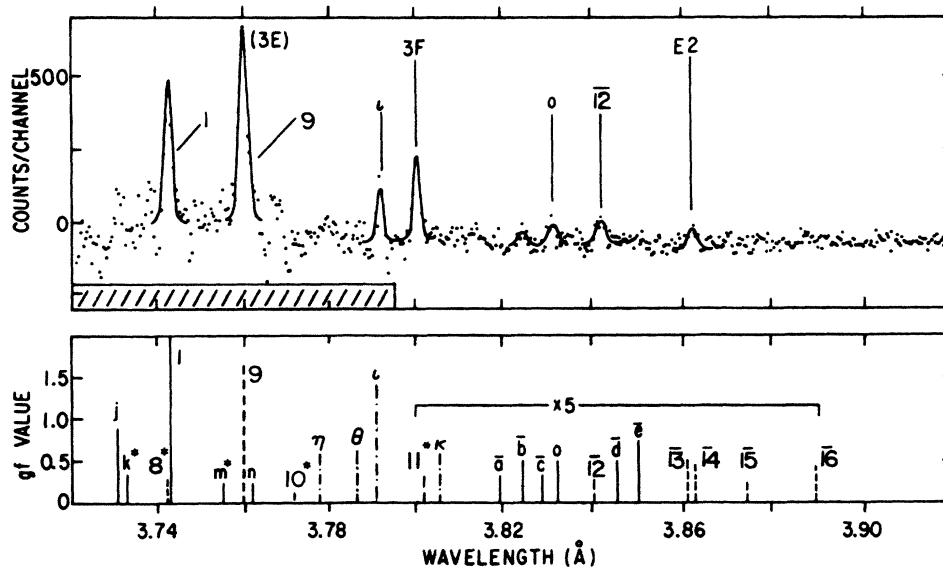


FIG. 13. Spectrum of silver in the wavelength region 3.720–3.920 Å. This region includes  $3d \rightarrow 2p$  and  $3s \rightarrow 2p$  transitions. The spectra of other impurities have been subtracted out for clarity. The hatched region indicates the location of the  $K\alpha$  spectrum of heliumlike iron. A theoretical spectrum containing sodiumlike, magnesiumlike, and aluminumlike transitions is shown below the experimental data. Neonlike transitions are labeled with upper-case letters; sodiumlike (solid), magnesiumlike (dashed), and aluminumlike (dot-dashed) lines are keyed with lower-case letters, with numbers, and with Greek letters, respectively.



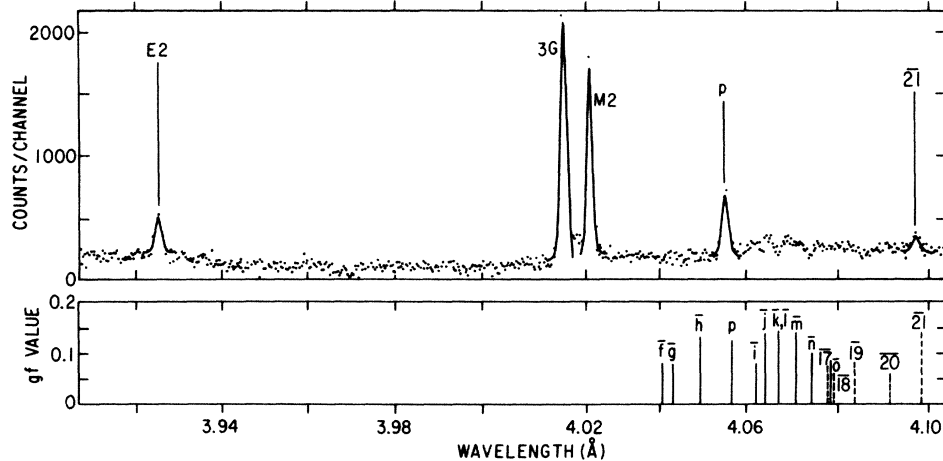


FIG. 14. Spectrum of silver in the wavelength region 3.910–4.100 Å. This region includes most of the  $3s \rightarrow 2p$  transitions. The spectra of other impurities have been subtracted out for clarity. A theoretical spectrum containing sodiumlike and magnesiumlike transitions is shown below the experimental data. Neonlike transitions are labeled with upper case letters; sodiumlike (solid) and magnesiumlike (dashed) lines are keyed with lower-case letters and with numbers, respectively.

of electrons in the  $n=3$  shell increases. For the neonlike charge state, however, we easily could take into account all configurations in the  $n=3$  and  $n=4$  complex.

In the next section we discuss the transitions in the neonlike charge state. Here we also describe a simple intensity calculation which we have used to corroborate the identifications of the weaker neonlike transitions. In the subsequent sections we identify the remaining strong features of the silver spectrum as particular transitions from the lower charge states.

#### A. Neonlike lines

The neonlike lines are the most readily identifiable  $M$ -to- $L$ -shell transitions. Looking at Figs. 11–14 the most prominent lines seen are the neonlike electric dipole transitions between the  $(2p^5 3s)_{J=1}$  and the  $(2p^5 3d)_{J=1}$  upper states and the  $(2p^6)_{J=0}$  ground state. These lines are labeled  $3C$ – $3G$ . These lines have also been the most prominent features in the spectra reported previously,<sup>1–15</sup> including the spectra of silver obtained by Burkhalter *et al.* from an exploding-wire plasma source<sup>10</sup> and by Aglitzki *et al.* from a low-inductance vacuum spark source.<sup>11</sup> One of the lines,  $3E$ , at  $\lambda=3.7598$  Å is labeled in parentheses; this line, the transition  $(2p^5_{3/2} 3d_{3/2})_{J=1}$  to the ground state, is predicted to be very weak, and the strong line seen is most likely due to the strong transition  $(2p^5_{3/2} 3s^2 3d_{5/2})_{J=1}$  to the ground state in magnesiumlike silver (see Sec. IV B 3). Two weaker electric dipole lines, labeled  $3A$  and  $3B$ , are also seen. These lines are due to the transitions from the  $(2s 2p^6 3p)_{J=1}$  upper states to the ground state.

Another prominent feature, seen in Fig. 14, is the magnetic quadrupole line, labeled  $M2$ , at  $\lambda=4.0245$  Å. It originates from the state  $(2p^5_{3/2} 3s_{1/2})_{J=2}$  which is the lowest excited state in neonlike silver. According to our calculations, the radiative decay rate of this state is  $6.0 \times 10^7$

$\text{sec}^{-1}$ . Hence, significant depopulation of this state by collisions occurs at electron densities above the threshold of approximately  $8 \times 10^{16} \text{ cm}^{-3}$ . Previous observations of neonlike silver<sup>10,11</sup> have been made from plasmas with electron densities above this value, and this transition has, therefore, not been observed. The  $M2$  transition has also not been observed in beamfoil experiments, since the ions move outside of the detection area before appreciable radiative decay takes place.

The features labeled  $E2$  in Figs. 12–14, which are situated at 3.6611, 3.8627, and 3.9250 Å, respectively, have been identified as the three forbidden electric quadrupole transitions from the  $(2p^5 3p)_{J=2}$  configuration to the ground state. These features are weak, and one is barely resolved from the background. Nevertheless, the lines have been observed consistently in each discharge with strong silver injection. We note that none of the  $E2$  lines is located in the spectral region dominated by line emission from other impurities in PLT plasmas (see Fig. 2). The observed intensities of these lines are also consistent with the values predicted by our modeling calculations, and we have checked for lines of other ions in this wavelength range. Transitions from fluorinelike silver or from lower charge states do not occur in the immediate vicinity of the  $E2$  transitions at 3.6611 and 3.9250 Å. Two very weak magnesiumlike lines (see features  $\bar{13}$  and  $\bar{14}$  in Fig. 13) are predicted near 3.8627 Å. Identification of the  $E2$  transition at this wavelength is, therefore, less certain.

The measured wavelengths of the neonlike transitions are listed in Table III. An error analysis similar to the one described in Sec. III yields an uncertainty of  $\pm 0.1$  mÅ. This corresponds to an accuracy of  $\Delta\lambda/\lambda=1/20000$  for most wavelengths. The uncertainty in the measured wavelengths of the two shortest  $E2$  transitions and of the line  $3B$  is higher due to the low number of counts. Their accuracy is estimated to be about four times less than that

for the other neonlike transitions. Most lines have been observed under various settings of the spectrometer, and the wavelengths measured at these different settings have been reproducible. As mentioned in Sec. III, we have used the theoretical wavelength value  $\lambda = 3.94921$  Å for line  $w$  of heliumlike argon<sup>31</sup> as a reference in the spectral range above 3.900 Å. For lines below 3.900 Å we have used the line  $w$  of heliumlike iron at  $\lambda = 1.85048$  Å as a reference.<sup>31</sup> Using the theoretical predictions by Mohr<sup>32</sup> for the Ly- $\alpha_1$  line of argon as a reference would shift our experimental values by 0.4 mÅ.

Table III also contains our *ab initio* wavelengths for the neonlike transitions. The agreement between the measured and calculated wavelengths for all neonlike lines is remarkably good. The agreement is found to be within 0.8 mÅ for most lines, including the quadrupole lines. The only exceptions are the two  $2s2p^63p \rightarrow 2s^22p^6$  transitions. They are measured to be longer by 1.5 and 1.0 mÅ, respectively, from the calculated value. These silver lines have the shortest wavelengths and are the furthest away from the line  $w$  of iron used as the wavelength reference. However, using the nearby  $K\beta$  line of argon as the wavelength reference, in general, does not change this result. It is interesting to note that all  $3p \rightarrow 2s$  and  $3d \rightarrow 2p$  transitions are measured to be of longer wavelength than predicted. The opposite is true for all  $3s \rightarrow 2p$  and  $3p \rightarrow 2p$  transitions, for which the measured values are shorter than predicted. In Table III we also list the wavelength values measured by Burkhalter *et al.*<sup>10</sup> and Aglitzki *et al.*<sup>11</sup> Our measurements agree with the values

obtained by Aglitzki *et al.* within the experimental error limits in the range from  $\Delta\lambda = \pm 0.5 - \pm 2.0$  mÅ cited in Ref. 11, except for line 3F. The values from the measurements by Burkhalter *et al.* differ considerably from ours and were taken with much smaller spectral resolution.

The spectra presented here offer the first simultaneous observation of both  $E2$  and  $M2$  transitions in any neonlike ion. Whereas the branching ratio for the  $M2$  transition, in the absence of collisions, is always unity, the branching ratios for the  $E2$  transitions approach unity only for high- $Z$  ions. At lower  $Z$ , the levels  $(2p^53p)_{J=2}$  decay instead by  $\Delta n = 0$  transitions to lower-lying excited states in the  $2p^53s$  configuration and cannot be observed. Neonlike iron spectra from tokamaks<sup>2</sup> and from the solar atmosphere<sup>12-15</sup> show a strong  $M2$ . The  $E2$  transitions, however, were not observed, since the branching ratio is not favorable due to the  $Z$  dependence in the decay rates. These lines have also not been observed in the spectra of neonlike molybdenum which has a  $Z$  of 42.<sup>4</sup> Observation of the  $E2$  lines has been reported so far only from beam-foil experiments involving neonlike and fluorinelike xenon.<sup>26</sup> Our observation of the  $E2$  transitions thus demonstrates that tokamaks are appropriate sources to study these transitions in high- $Z$  neonlike ions.

Observation of the  $3p \rightarrow 2p$  electric quadrupole transitions, in addition to the electric dipole transitions, allows a determination of the  $\Delta n = 0$  transition energies between states of opposite parity. Some of the possible  $\Delta n = 0$  transitions are shown in the Grotrian diagram in Fig. 15, and the corresponding wavelengths are listed in Table IV.

TABLE III. Comparison of experimental and calculated wavelengths for  $n=3$  to  $n=2$  transitions in neonlike silver. The upper level is designated in  $(j_1, j_2)_J$  notation. The theoretical values for the line intensities have been calculated assuming an electron temperature of 3 keV and a density of  $3 \times 10^{13} \text{ cm}^{-3}$ .

Upper Level	Key	$\lambda_{\text{theor}}$ (Å)	$\lambda_{\text{expt}}^a$ (Å)	$\lambda_{\text{expt}}^b$ (Å)	$\lambda_{\text{expt}}^c$ (Å)	Intensity (calc)	Intensity (expt <sup>a</sup> )
$2s2p^63p$							
$(1/2, 3/2)_1$	3A	3.3989	3.4004		3.3983	0.08	0.29
$(1/2, 1/2)_1$	3B	3.4448	3.4458	3.465	3.444	0.04	0.07
$2s^22p^53d$							
$(1/2, 3/2)_1$	3C	3.5466	3.5467	3.557	3.5474	1.00	1.00
$(3/2, 5/2)_1$	3D	3.7177	3.7179	3.732	3.7181	1.58	1.50
$(3/2, 3/2)_1$	3E	3.7607	3.7598 <sup>d</sup>	3.760		0.02	0.58 <sup>d</sup>
$2s^22p^53p$							
$(1/2, 3/2)_2$	E2	3.6619	3.6611			0.04	0.06
$(3/2, 3/2)_2$	E2	3.8631	3.8627			0.06	0.05
$(3/2, 1/2)_2$	E2	3.9253	3.9250			0.13	0.09
$2s^22p^53s$							
$(1/2, 1/2)_1$	3F	3.8005	3.8003	3.825	3.8023	0.33	0.43
$(3/2, 1/2)_1$	3G	4.0192	4.0186	4.031	4.0186	0.93	0.74
$(3/2, 1/2)_2$	M2	4.0253	4.0245			0.35	0.54

<sup>a</sup>Present measurement; lines with wavelength  $\lambda \leq 3.90$  Å are referenced to line  $w$  of iron; those with  $\lambda \geq 3.90$  Å are referenced to line  $w$  of argon.

<sup>b</sup>Reference 10.

<sup>c</sup>Reference 11.

<sup>d</sup>Line blended with magnesiumlike line.

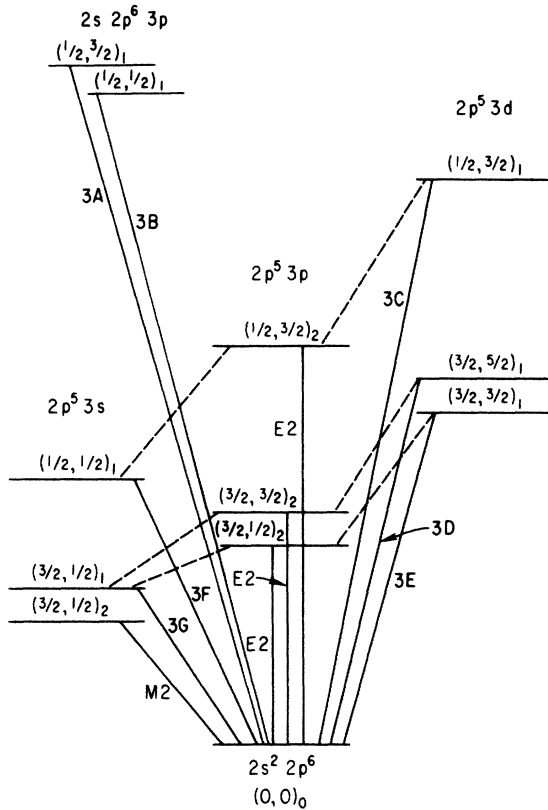


FIG. 15. Grotrian diagram of selected energy levels and transitions in  $\text{Ag}^{37+}$ . The solid lines represent the  $\Delta n=1$  radiative transitions listed in Table III. The dashed lines indicate some of the possible  $\Delta n=0$  intrashell radiative transitions which are listed in Table IV. The energy levels are designated using  $jj$ -coupling, i.e.,  $(j_1, j_2)_J$ , where  $j_1$ ,  $j_2$ , and  $J$  are the angular momentum of the hole state and the excited state, and the total angular momentum, respectively.

These transitions have become of great interest in the development of soft-x-ray lasers.<sup>45</sup> Here amplification and lasing were achieved for the  $\Delta n=0$  transitions  $(2p_{1/2}^5 3p_{3/2})_{J=2} \rightarrow (2p_{1/2}^5 3s_{1/2})_{J=1}$  and  $(2p_{3/2}^5 3p_{3/2})_{J=2} \rightarrow (2p_{3/2}^5 3s_{1/2})_{J=1}$  in selenium.<sup>24,25</sup> Identification of these lines from direct observations in the extreme vacuum uv and soft-x-ray region is difficult due to the pres-

ence of many lines of almost identical wavelengths which result from stronger  $\Delta n=0$  transitions in atoms of adjacent charge states. Achieving gain in a silver target in a similar experiment could reduce the laser output wavelengths from approximately 200 to 100 Å.

In Table III we have also listed the measured and calculated values for the intensities of the neonlike transitions. The intensities are normalized to the intensity of the line 3C. Whereas we have been able to measure the wavelengths with very high accuracy, the measured intensity ratios are much less reliable. In order to evaluate the line intensity ratios for the entire spectral range, lines common to spectra obtained with different settings of the spectrometer have been used for normalization. However, different settings of the spectrometer also correspond to PLT discharges from different run days. The variations in the plasma conditions which may have occurred for different run days thus make it difficult to determine these line ratios with high accuracy. The intensity data in Table III were obtained from discharges with electron temperatures ranging from approximately 2.6 to 3.1 keV. No adjustments have been made to account for the variations in the response of the spectrometer to different wavelengths, e.g., the wavelength dependence of the crystal reflectivity and the detection efficiency of the multiwire proportional counter have not been considered. However, corrections for the absorption properties of the helium and the beryllium windows (Fig. 1) and corrections for the vignetting of some of the spectral lines by the PLT port and the lead apertures were made. The intensity ratios for lines that are far apart are, therefore, less reliable than the intensity ratios of lines that are next to each other.

The theoretical values for the line intensities have been obtained from a collisional radiative equilibrium model calculation. This model is similar to the one originally used by Louergue and Nussbaumer for iron;<sup>19</sup> it contains processes among the ground state and the lowest 36 excited states in neonlike silver. These excited states correspond to configurations with an electron in the  $n=3$  shell and a hole in the  $n=2$  shell. For the densities in the PLT plasmas we only need to include collisions from the ground state and not from the excited states. We consider all  $\Delta n=0$  and  $\Delta n=1$  electric dipole radiative cascades with levels  $n=3$ . We also include the contributions from

TABLE IV. Comparison of experimental and theoretical  $\Delta n=0$  intervals in  $\text{Ag}^{37+}$ . The levels are designated in  $(j_1, j_2)_J$  notation.

Transition	Energy (expt) (eV)	Energy (theor) (eV)
$1s^2 2s^2 2p^5 3p \rightarrow 1s^2 2s^2 2p^5 3s$		
$(3/2, 1/2)_2 \rightarrow (3/2, 1/2)_1$	73.6	73.8
$(3/2, 3/2)_2 \rightarrow (3/2, 1/2)_1$	124.5	124.7
$(1/2, 3/2)_2 \rightarrow (1/2, 1/2)_1$	124.1	123.5
$1s^2 2s^2 2p^5 3d \rightarrow 1s^2 2s^2 2p^5 3p$		
$(3/2, 3/2)_1 \rightarrow (3/2, 1/2)_2$	109.2	110.0
$(3/2, 5/2)_1 \rightarrow (3/2, 3/2)_2$	125.0	125.5
$(1/2, 3/2)_1 \rightarrow (1/2, 3/2)_2$	a	138.2

<sup>a</sup>Upper level blended with magnesiumlike transition.

the  $E2$  and  $M2$  forbidden transitions to the ground state, and the  $\Delta n=0$   $M1$  transition from the  $J=0$  to the  $J=1$  level in the  $2p^5 3s$  configuration.

All energy levels and  $E1$  transition rates are obtained from the RAC calculations. The rates for the forbidden transitions have been supplied from a similar set of atomic physics codes which use orbitals generated by the Grant multiconfiguration Dirac-Fock (MCDF) program.<sup>46,47</sup> The electron-impact ground-state excitation rates are obtained from a third set of atomic physics codes which perform relativistic distorted-wave calculations for the cross sections.<sup>48</sup> The largest excitation rate coefficients are listed in Table V. It is interesting to note that collisional excitation from the ground state predominantly populates the levels  $(2p_{3/2}^5 3d_{5/2})_{J=1}$ ,  $(2p_{1/2}^5 3d_{3/2})_{J=1}$ ,  $(2p_{3/2}^5 3p_{3/2})_{J=0}$ , and  $(2p_{1/2}^5 3p_{1/2})_{J=0}$ . These four levels receive approximately 70% of all flux from the ground state. The other levels, notably the  $2p^5 3s$ , levels, are populated by  $\Delta n=0$  radiative cascades.

The theoretical line intensities listed in Table III have been calculated for an electron temperature of 3 keV and density of  $3 \times 10^{13} \text{ cm}^{-3}$ . Despite the shortcomings of both the measurements and our simple model, the experimental and predicted intensity ratios are in general agreement. For example, the observed intensities of the weak  $E2$  lines and of the strong  $3d \rightarrow 2p$  transitions are consistent with the strength predicted. A notable exception, however, is the transition  $3E$  from  $(2p_{3/2}^5 3d_{3/2})_{J=1}$  to ground. The intensity of the feature observed at 3.7598 Å is 30 times larger than the value predicted for the transition  $3E$ . This indicates that this feature is composed of several lines, and is most likely due to a strong  $3d \rightarrow 2p$  transition in magnesiumlike silver, as discussed below. Discrepancies between the observed and the theoretical values also exist for some other lines. As an example, we consider the intensity ratio of the lines  $M2$  and  $3G$  at  $\lambda=4.0245$  and  $4.0186$  Å, respectively. The two lines are strong and very close to each other so that the measured intensity ratio is very reliable. The predicted intensity ratio, however, differs from the observed value by a factor of 2. A similar discrepancy for the ratio of the two lines

TABLE V. Direct ground-state excitation rate coefficients for  $\text{Ag}^{37+}$ . Only levels that receive more than 2% of the excitation flux from the ground state are listed. The values are calculated for an electron temperature of 3 keV and density of  $3 \times 10^{13} \text{ cm}^{-3}$ .

Level	Rate coefficient ( $\text{cm}^3/\text{sec}$ )	Fraction of total flux from ground state
$(2p_{3/2}^5 3d_{5/2})_1$	$1.55 \times 10^{-11}$	0.34
$(2p_{1/2}^5 3d_{3/2})_1$	$1.01 \times 10^{-11}$	0.22
$(2p_{3/2}^5 3p_{3/2})_0$	$3.46 \times 10^{-12}$	0.07
$(2p_{1/2}^5 3p_{1/2})_0$	$3.32 \times 10^{-12}$	0.07
$(2s_{1/2} 3d_{5/2})_2$	$2.55 \times 10^{-12}$	0.06
$(2s_{1/2} 3s_{1/2})_0$	$2.33 \times 10^{-12}$	0.05
$(2s_{1/2} 3p_{3/2})_1$	$7.15 \times 10^{-13}$	0.02

has been observed for neonlike iron in solar flare spectra,<sup>12–15</sup> where again the  $M2$  line was found to be much larger than predicted by the model of Loulergue and Nussbaumer.<sup>19,44</sup>

Several, possibly important, processes are missing from our model. First, we note the absence of radiative cascades from states with principal quantum number higher than  $n=3$ .<sup>44</sup> The contributions from cascades should be more important at higher temperatures. We have also not included resonances in the cross sections, such as those discussed recently<sup>49</sup> in the case of neonlike iron; at a sufficiently low temperature, these can cause additional populations among the  $2p^5 3s$  levels. An equally, if not more likely, process than either of the previous two processes may be the ionization of a  $2p$  electron from the  $2p^6 3s$  ground state of the sodiumlike ion. This process is also missing from our model and may be important especially because of the large abundance of sodiumlike ions in the plasma as evidenced by the presence of strong sodiumlike lines in the spectrum. The process also enhances the population of the neonlike  $2p^5 3s$  levels and might in particular explain the strong intensity of the  $M2$  line. This is yet an additional suggestion that the populations of neighboring charge states may have an observable influence in populating the excited states in the neonlike ion.<sup>50</sup>

## B. Lines from lower charge states

Whereas a neonlike ion has the relatively modest number of 36 singly excited states with a hole in the  $n=2$  shell and a single electron in the  $n=3$  shell, a sodiumlike ion has 237 excited states with the same vacancy in the  $n=2$  shell, but with two  $n=3$  electrons. For magnesiumlike ions there are three  $n=3$  excited electrons, and for aluminumlike ions there are four; the complexity of these ions is therefore considerably greater. These states are different from the singly excited states of neonlike silver because they are autoionizing states. As a result they can decay spontaneously by autoionization in addition to the normal radiative channels, and they can be populated directly by dielectronic capture. However, similar to the neonlike states they can be formed by the collisional excitation of an electron from the  $n=2$  shell. For the low densities in the PLT, nearly all ions of each charge state are in the ground states.

For this paper, we have not calculated intensities based on all these processes. Instead we have tried to identify the lines of the lower charge states by combining calculations of oscillator strengths from the RAC code with some qualitative understanding of excitation mechanisms. Most importantly, we have looked for transitions which are analogues to transitions in the neonlike ions. For example, our calculations of the excitation processes in neonlike silver predict that the strongest excitations from the ground state proceed via  $2p \rightarrow 3d$  dipole excitations (see Table V). Hence we expect that the same type of dipole-allowed excitations will produce some of the strongest lines from each lower charge state. The strength of these transitions can then be used as an indicator as to whether lines of a certain charge state are present in the spectral range investigated. For example, if none of the

$3d \rightarrow 2p$  transitions of a certain charge state can be identified in the spectrum, we assume that no lines from this ion are present. In this way we can narrow down the number of charge states which contribute to our spectrum. For the remaining charge states we then also look for states which can be populated by the strongest of the direct nondipole excitations or by arbitrary cascades from higher states. We also consider the fact that the population of some states may be enhanced via inner-shell ionization of the adjacent lower charge state.

The most difficult transitions to consider are those produced by dielectronic recombination. In the case of sodiumlike silver we have an explicit calculation of the dielectronic recombination spectrum. The results of this calculation, which are presented in Sec. IV B 2, indicate that the contribution of dielectronic recombination to the spectrum of sodiumlike silver is weak at an electron temperature of 3 keV. Unfortunately, we cannot assume the same about subsequent charge states without performing further calculations. However, the results of the calculations for sodiumlike silver suggest that the configurations, which should be populated the most by this process, are states with high total angular momentum corresponding to a  $2p \rightarrow 3d$  excitation and simultaneous capture of an electron into a  $3d$  orbital. Such configurations are not populated directly either by excitation or ionization from the ground state. Hence, if transitions from these configurations were observed, they could provide some measure of the magnitude of dielectronic recombination. In the remaining part of this section we summarize the identifications for each of the lower charge states observed.

### 1. Sodiumlike lines

In addition to the transitions  $3d \rightarrow 2p$  ( $3s$  spectator) which we have used as an indicator for the presence of the sodiumlike charge state, we have also considered the transitions of the type  $3s \rightarrow 2p$  ( $3d$  spectator),  $3s \rightarrow 2p$  ( $3p$  spectator),  $3s \rightarrow 2p$  ( $3s$  spectator), and  $3p \rightarrow 2s$  ( $3s$  spectator). Three of these types are analogous to the strong  $E1$  transitions in neonlike ions, and we expect them to be strong in the sodiumlike ion. We expect the other two types of transitions,  $3s \rightarrow 2p$  ( $3d$  spectator) and  $3s \rightarrow 2p$  ( $3p$  spectator) to be weaker: the first type, because it has to compete with the strong transition type  $3d \rightarrow 2p$  ( $3s$  spectator); the second, because its upper level is analogous to the comparatively weakly populated  $2p^5 3p$  excited level in neonlike ions. The wavelengths of the particular transitions with  $gf$  values, i.e., the product of the statistical weight  $g$  of the lower level and the absorption oscillator strength  $f$  of the transition, larger than 0.06 are listed in Table VI. They have also been plotted as solid lines in Figs. 11–14 and are labeled with lower case letters. Although all upper levels of the transitions  $3d \rightarrow 2p$  are mixtures of states of the type  $2p^5 3s 3d$  and  $2p^5 3p^2$ , we have used only the dominant contribution to denote the upper level. If the dominant contribution of these mixed states is from the  $2p^5 3p^2$  configuration, we have added a superscript asterisk to the key. Any transition from these states to the ground state occurs only because the upper level includes an admixture of the  $2p^5 3s 3d$  configuration.

The three strongest sodium-like lines have been identified as transitions of the type  $3d \rightarrow 2p$ , as expected. They are situated to the long-wavelength side of the  $3d \rightarrow 2p$  neonlike lines  $3C$  and  $3D$  and are labeled f, h, and l, respectively. A fourth line j is also predicted to have a large  $gf$  value. However, this transition falls into the region dominated by the iron  $K\alpha$  spectrum (see Fig. 10), and our identification of the line in the experimental data is not conclusive. Similarly, all  $3d \rightarrow 2p$  transitions whose upper level is dominated by  $2p^5 3p^2$  states are blended with other strong silver lines. Thus no experimental evidence exists on the strength of these transitions. The theoretically predicted  $gf$  values for these lines are, however, smaller than those for the transitions f, h, and l. Two of these lines, e\* and i\*, with  $gf$  values of 0.52 and 0.29, respectively, are predicted to be blended with the neonlike transitions  $3C$  and  $3D$ , respectively. If these lines were stronger than predicted, then they could possibly cause a shift in the apparent wavelength of the neonlike lines.

The two transitions  $2p^5 3s^2 \rightarrow 2p^6 3s$  which are analogues to the neonlike lines  $3F$  and  $3G$  are also observed. The lines are labeled o and p and are seen in Figs. 13 and 14, respectively. These lines may be excited not only via  $\Delta n=0$  cascading, but also by inner-shell ionization of magnesiumlike ions in the ground state. Furthermore, we have observed two sodiumlike lines labeled a and b which are of the type  $3p \rightarrow 2s$  ( $3s$  spectator). The lines are weak in agreement with their predicted  $gf$  value and occur on the long-wavelength side of the neonlike line  $3A$ . Two other sodiumlike transitions labeled c and d, which occur on the long-wavelength side of the neonlike line  $3B$  have smaller  $g$  values and have not been observed.

We have labeled all the remaining transitions in Table VI with an overbar. These transitions are of the type  $3s \rightarrow 2p$  ( $3p$  or  $3d$  spectator). The wavelengths listed in Table VI indicate that these transitions are clustered together in two regions of the spectrum: between  $3.82 \leq \lambda \leq 3.85$  Å, around line o, and between  $4.04 \leq \lambda \leq 4.08$  Å, around line p. Although we have not been able to identify any individual line, these transitions could account for the structure in the spectrum seen to either side of line p at  $\lambda=4.0547$  Å. Similarly, lines  $\bar{a}$ – $\bar{e}$  could perhaps contribute to the two features in the data to the long- and short-wavelength sides of line o at  $\lambda=3.8309$  Å. Unambiguous identifications, however, are difficult without a better signal-to-noise ratio.

### 2. Dielectronic lines

A calculation of the dielectronic recombination spectrum for the sodiumlike charge state was performed, in order to check the importance of this process. Dielectronic recombination does not contribute to the excitation of the neonlike lines due to the small abundance of fluorine-like ions in the plasma; it could, however, be relevant for the sodiumlike spectrum, since the abundance of neonlike ions is clearly large. Dielectronic recombination tends to populate different configurations than those populated by direct excitation or inner-shell ionization. In order to compute the resulting line intensities, we have calculated

the autoionization and radiative rates for all the 237 excited states with two electrons in the  $n=3$  shell.<sup>47</sup>

The eight strongest sodiumlike dielectronic lines are listed in Table VII. These lines are found on the long-wavelength side of the lines 3C and 3D. Our calculations indicate that at a 3-keV electron temperature the strongest satellite, at  $\lambda=3.7469$  Å, should have only about 5% of the intensity predicted for line 3D. (Note that this ratio is

independent of the relative abundance of the neonlike and sodiumlike ions.) Thus we expect that these satellites are weak compared to the intensity of the neonlike lines. Indeed, no significant intensities are experimentally observed at the wavelengths predicted for these lines. For example, consider the wavelength region from 3.54 to 3.59 Å near the line 3C in Fig. 12. This region is predicted to contain three of the eight satellites listed in Table VII. If

TABLE VI. Experimental wavelengths and theoretical predictions for  $n=3$  to  $n=2$  transitions in sodiumlike silver. Only transitions with  $gf$  values larger than 0.06 are listed. gs denotes the ground state, bl a line blended with a strong line, ur an unresolved line due to the  $K\alpha$  spectrum of iron, and  $\langle \rangle$  the average wavelength of several unresolved lines.

Transition	Key	$\lambda_{\text{expt}}^a$ (Å)	$\lambda_{\text{theor}}$ (Å)	$gf$
<b>3p → 2s (3s spectator)</b>				
$(2s_{1/2}2p^63s_{1/2}3p_{1/2})_{3/2} \rightarrow \text{gs}$	a	3.412	3.4103	0.14
$(2s_{1/2}2p^63s_{1/2}3p_{1/2})_{1/2} \rightarrow \text{gs}$	b	3.426	3.4249	0.43
$(2s_{1/2}2p^63s_{1/2}3p_{3/2})_{3/2} \rightarrow \text{gs}$	c		3.4586	0.11
$(2s_{1/2}2p^63s_{1/2}3p_{3/2})_{1/2} \rightarrow \text{gs}$	d		3.4726	0.09
<b>3d → 2p (3s spectator)</b>				
$(2p_{1/2}^53p_{3/2}3p_{3/2})_{3/2} \rightarrow \text{gs}$	e*	bl	3.5446	0.52
$(2p_{1/2}^53s_{1/2}3d_{3/2})_{1/2} \rightarrow \text{gs}$	f	$\langle 3.571 \rangle$	3.5705	1.03
$(2p_{1/2}^53p_{3/2}3p_{3/2})_{3/2} \rightarrow \text{gs}$	g*	$\langle 3.571 \rangle$	3.5707	0.50
$(2p_{1/2}^53s_{1/2}3d_{5/2})_{3/2} \rightarrow \text{gs}$	h	$\langle 3.571 \rangle$	3.5729	0.94
$(2p_{3/2}^53p_{3/2}3p_{3/2})_{3/2} \rightarrow \text{gs}$	i*	bl	3.7178	0.29
$(2p_{3/2}^53s_{1/2}3d_{3/2})_{1/2} \rightarrow \text{gs}$	j	ur	3.7308	0.92
$(2p_{3/2}^53p_{3/2}3p_{3/2})_{3/2} \rightarrow \text{gs}$	k*	ur	3.7333	0.27
$(2p_{3/2}^53s_{1/2}3d_{5/2})_{3/2} \rightarrow \text{gs}$	l	3.7427	3.7431	2.14
$(2p_{3/2}^53p_{3/2}3p_{3/2})_{1/2} \rightarrow \text{gs}$	m*	bl	3.7566	0.21
$(2p_{3/2}^53s_{1/2}3d_{3/2})_{1/2} \rightarrow \text{gs}$	n	ur	3.7623	0.20
<b>3s → 2p (3s spectator)</b>				
$(2p_{1/2}^53s^2)_{1/2} \rightarrow \text{gs}$	o	3.8309	3.8325	0.08
$(2p_{3/2}^53s^2)_{3/2} \rightarrow \text{gs}$	p	4.0547	4.0570	0.12
<b>3s → 2p (3p spectator)</b>				
$(2p_{1/2}^53s_{1/2}3p_{1/2})_{1/2} \rightarrow 2p^63p_{1/2}$	$\bar{a}$		3.8190	0.06
$(2p_{1/2}^53s_{1/2}3p_{3/2})_{3/2} \rightarrow 2p^63p_{3/2}$	$\bar{b}$		3.8245	0.09
$(2p_{1/2}^53s_{1/2}3p_{1/2})_{3/2} \rightarrow 2p^63p_{1/2}$	$\bar{d}$		3.8462	0.10
$(2p_{1/2}^53s_{1/2}3p_{3/2})_{5/2} \rightarrow 2p^63p_{3/2}$	$\bar{e}$		3.8508	0.15
$(2p_{3/2}^53s_{1/2}3p_{3/2})_{3/2} \rightarrow 2p^63p_{3/2}$	$\bar{g}$		4.0438	0.08
$(2p_{3/2}^53s_{1/2}3p_{3/2})_{5/2} \rightarrow 2p^63p_{3/2}$	$\bar{h}$		4.0495	0.13
$(2p_{3/2}^53s_{1/2}3p_{3/2})_{1/2} \rightarrow 2p^63p_{3/2}$	$\bar{k}$		4.0674	0.06
$(2p_{3/2}^53s_{1/2}3p_{1/2})_{1/2} \rightarrow 2p^63p_{1/2}$	$\bar{l}$		4.0677	0.07
$(2p_{3/2}^53s_{1/2}3p_{1/2})_{3/2} \rightarrow 2p^63p_{1/2}$	$\bar{m}$		4.0708	0.14
$(2p_{3/2}^53s_{1/2}3p_{3/2})_{5/2} \rightarrow 2p^63p_{3/2}$	$\bar{n}$		4.0747	0.10
$(2p_{3/2}^53s_{1/2}3p_{3/2})_{3/2} \rightarrow 2p^63p_{3/2}$	$\bar{o}$		4.0781	0.09
<b>3s → 2p (3d spectator)</b>				
$(2p_{1/2}^53s_{1/2}3d_{3/2})_{1/2} \rightarrow 2p^63d_{3/2}$	$\bar{c}$		3.8288	0.06
$(2p_{3/2}^53s_{1/2}3d_{5/2})_{3/2} \rightarrow 2p^63d_{5/2}$	$\bar{f}$		4.0407	0.08
$(2p_{3/2}^53s_{1/2}3d_{5/2})_{3/2} \rightarrow 2p^63d_{5/2}$	$\bar{i}$		4.0621	0.08
$(2p_{3/2}^53s_{1/2}3d_{3/2})_{3/2} \rightarrow 2p^63d_{3/2}$	$\bar{j}$		4.0640	0.13

<sup>a</sup>Lines with wavelength  $\lambda \leq 3.90$  Å are referenced to the line  $w$  of iron; those with  $\lambda \geq 3.90$  Å are referenced to the line  $w$  of argon.

TABLE VII. Atomic data and relative intensities of the eight strongest dielectronic satellites of neonlike silver. The intensity of the strongest satellite is about 5% of the intensity of the neonlike  $3D$  line at 3 keV. The radiative transition probability  $A_r$  and the autoionization probability  $A_a$  are given in  $10^{14} \text{ s}^{-1}$ .  $\omega$  denotes the fluorescence yield.

Transition	$\lambda$ ( $\text{\AA}$ )	Relative intensity	$A_r$	$A_a$	$\omega$
$(2p^5_{3/2}3d_{3/2}3d_{5/2})_{5/2} \rightarrow (2p^6_{3/2}3d_{3/2})_{3/2}$	3.7469	1.00	2.7	7.5	0.26
$(2p^5_{1/2}3d_{3/2}3d_{5/2})_{7/2} \rightarrow (2p^6_{3/2}3d_{5/2})_{5/2}$	3.5688	0.85	1.9	4.0	0.32
$(2p^5_{3/2}3d_{5/2}3d_{5/2})_{7/2} \rightarrow (2p^6_{3/2}3d_{5/2})_{5/2}$	3.7528	0.67	1.5	2.9	0.33
$(2p^5_{1/2}3p_{3/2}3d_{3/2})_{5/2} \rightarrow (2p^6_{3/2}3p_{3/2})_{3/2}$	3.5583	0.39	1.4	1.6	0.47
$(2p^5_{3/2}3p_{3/2}3d_{5/2})_{3/2} \rightarrow (2p^6_{3/2}3p_{3/2})_{3/2}$	3.7388	0.31	1.5	2.0	0.43
$(2p^5_{3/2}3p_{3/2}3d_{5/2})_{5/2} \rightarrow (2p^6_{3/2}3p_{3/2})_{3/2}$	3.7522	0.21	1.1	0.6	0.64
$(2p^5_{1/2}3d_{3/2}3d_{3/2})_{5/2} \rightarrow (2p^6_{3/2}3d_{3/2})_{3/2}$	3.5898	0.21	0.7	1.1	0.36
$(2p^5_{3/2}3p_{3/2}3d_{5/2})_{5/2} \rightarrow (2p^6_{3/2}3p_{3/2})_{3/2}$	3.7387	0.20	1.8	0.5	0.79

the satellite predicted for  $\lambda = 3.5688 \text{ \AA}$  were to contribute significantly to the feature labeled f and h at 3.567–3.575  $\text{\AA}$ , then we would expect to be able to identify the relatively strong satellite predicted for  $\lambda = 3.5583 \text{ \AA}$ . The spectrum, however, does not show a feature near this wavelength. Since the intensity of the satellite at  $\lambda = 3.5583 \text{ \AA}$  is predicted to be only 3% of the strength of the line 3C, a very improved signal-to-noise ratio is needed to identify such a weak feature.

### 3. Magnesiumlike lines

The magnesiumlike ground state  $(2p^63s^2)_{J=0}$  contains the neonlike core with a closed  $3s$  subshell. Since the  $3s^2$  spectator electrons contribute no additional angular momentum, the excited states formed by the excitation of an electron from the  $n=2$  shell in the magnesiumlike ion are very similar to the neonlike excited states. The excited states in magnesiumlike ions thus correspond almost exactly to a subset of the neonlike states, with the lowest being the state  $2p^53s^23p$ .

The list of magnesiumlike transitions we have looked for is given in Table VIII. Again only lines with a  $gf$  value larger than 0.06 are included. The lines are plotted in Figs. 11–14 as dashed lines and are labeled 1–21. As in the case for the neonlike and sodiumlike ions, the transitions produced by a direct  $2p \rightarrow 3d$  excitation have the largest  $gf$  value and can be easily identified in the observed spectra as lines 5 and 9 in Figs. 12 and 13. These lines are close analogues to the neonlike lines 3C and 3D, respectively. Observing transitions of the type  $2p^53s^23d \rightarrow 2p^63s3d$  is not as likely because the branching ratios are less favorable. As in the sodiumlike sequence, there is significant configuration mixing of the  $3s3d$  and  $3p^2$  orbitals. In Table VIII transitions whose upper level is dominated by a  $2p^53s3p^2$  state are again labeled with a superscript asterisk. These lines have a smaller  $gf$  value than those whose upper level is dominated by a  $3s^23d$  state. All of these lines except possibly the lines 6\* and 7\* are blended with stronger lines, as is the case for the sodiumlike lines of this type, and none have been identified.

Two lines are listed in Table VIII which are transitions of the type  $3p \rightarrow 2s$ , lines 1 and 2. The lines are close analogues to the neonlike lines 3A and 3B. The stronger of these may possibly be identified as the weak line on the short-wavelength side of line 3B in Fig. 11. Seven lines are listed in Table VIII which are of the type  $3s \rightarrow 2p$  ( $3s3p$  spectator) and are labeled with an overbar. The two lines  $\bar{13}$  and  $\bar{14}$  at 3.8609 and 3.8624  $\text{\AA}$ , respectively, are predicted to occur close to the neonlike  $E2$  line at 3.8627  $\text{\AA}$  and could possibly blend in with this line. However, the lines  $\bar{15}$ ,  $\bar{16}$ ,  $\bar{19}$ , and  $\bar{20}$ , which have similarly small  $gf$  values and presumably similar population mechanisms as the lines  $\bar{13}$  and  $\bar{14}$ , are absent. Hence, we presume that the lines  $\bar{13}$  and  $\bar{14}$  are negligibly small as well and that the line seen at 3.8627  $\text{\AA}$  is truly the neonlike electric quadrupole line. The feature seen at 3.8425  $\text{\AA}$  has been tentatively ascribed to the transition  $\bar{12}$ , despite its very small  $gf$  value listed in Table VII. We do this because of the analogy to neonlike systems where monopole excitation from the ground state to the upper level  $(2p^5_{1/2}3p_{1/2})_{J=0}$  is strong (see Table V). For the neonlike level, radiative decay of the  $3p$  electron to the ground state is strictly forbidden; for the magnesiumlike level, however, one of the two  $3s$  electrons can make a radiative transition to the  $2p$  vacancy. Line  $\bar{12}$  may be evidence for such a process. The neonlike level  $(2p^5_{1/2}3p_{1/2})_{J=0}$  has been of great importance in the development of soft-x-ray lasers. The  $\Delta n=0$  transition between this level and the level  $(2p^5_{1/2}3s_{1/2})_{J=1}$  was predicted to exhibit the largest gain.<sup>24</sup> However, this transition has shown only weak gain. Hence further studies of the analogous upper level of line  $\bar{12}$  in magnesiumlike systems may shed light on the discrepancies noted in neonlike systems. The second magnesiumlike line of this kind, labeled  $\bar{18}$ , with upper level  $(2p^5_{3/2}3p_{3/2})_{J=0}$  is predicted at 4.0784  $\text{\AA}$ . At this wavelength, however, no clear feature is seen in our data which can be ascribed to this transition. The feature at  $\lambda = 4.0965 \text{ \AA}$  has been tentatively ascribed to the transition labeled  $\bar{21}$ , since this transition may not only be excited via electric quadrupole excitation from the ground state, as some of the other transitions of this type, but it

may also be excited via inner-shell ionization of the aluminumlike ground state  $2p^6 3s^2 3p_{1/2} \rightarrow 2p^5 3s^2 3p_{1/2}$ , similar to the neighboring sodiumlike line  $p$  and the neonlike transition  $3G$ .

#### 4. Aluminumlike lines

We expect to find evidence of aluminumlike transitions in our spectra, as aluminumlike ions exist in the colder, outer regions of the plasma which surround the hot core containing the neonlike and the sodiumlike ions. Table IX lists ten transitions which are analogous to the strongest transitions in the adjacent higher ionization states. These lines are plotted as dot-dashed lines in Figs. 11–14 and are labeled with lower-case Greek letters. The accuracy of the wavelength predictions is lower for the aluminumlike transitions than for the neonlike lines due to the large increase of interacting energy levels as one proceeds from the high to the low charge states. The accuracy of the aluminumlike wavelengths is estimated to be only  $\pm 5$  mÅ compared to a five times better accuracy for the neonlike wavelengths. Nevertheless, the dominant transi-

tions of the type  $3d \rightarrow 2p$  have been easily identified, and the calculated and measured wavelengths differ from each other by no more than 1 mÅ.

Our scheme of line identification seems successful in accounting for all features seen in the data. One exception, though, is the line at 3.4320 Å in Fig. 11. Although clearly a result of the silver injection into the plasma, this line remains unidentified. One candidate is a magnetic quadrupole transition in the magnesiumlike ion, the transition  $(2s_{1/2} 2p^6 3s^2 3p_{3/2})_{J=2}$  to the ground state. However, its wavelength is predicted to occur at 3.448 Å, which is much too long. Also, the strongest fluorinelike lines, again transitions of the type  $3d \rightarrow 2p$ , are predicted to occur at 3.6138, 3.4575, and 3.6323 Å with  $gf$  values of 2.73, 2.27, and 1.99, respectively. However, these lines are not observed. Another possibility might be the presence of a magnesiumlike dielectronic satellite line.

#### V. CONCLUSIONS

The emphasis of this paper has been to identify the features observed in a neonlike spectrum of a high- $Z$  ele-

TABLE VIII. Experimental wavelengths and theoretical predictions for  $n=3$  to  $n=2$  transitions in magnesiumlike silver. Only transitions with  $gf$  values larger than 0.06 are listed.  $gs$  denotes the ground state,  $bl$  a line blended with a strong line, and  $ur$  an unresolved line due to the  $K\alpha$  spectrum of iron.

Transition	Key	$\lambda_{\text{expt}}^a$ (Å)	$\lambda_{\text{theor}}$ (Å)	$gf$
$3p \rightarrow 2s$ ( $3s^2$ spectators)				
$(2s_{1/2} 2p^6 3s^2 3p_{3/2})_1 \rightarrow gs$	1	3.444	3.4399	0.28
$(2s_{1/2} 2p^6 3s^2 3p_{1/2})_1 \rightarrow gs$	2		3.4859	0.09
$3d \rightarrow 2p$ ( $3s^2$ spectators)				
$(2p_{1/2}^5 3s_{1/2} 3p_{3/2} 3p_{3/2})_1 \rightarrow gs$	3*	bl	3.5734	0.13
$(2p_{1/2}^5 3s_{1/2} 3p_{3/2} 3p_{3/2})_1 \rightarrow gs$	4*	bl	3.5738	0.23
$(2p_{1/2}^5 3s^2 3d_{3/2})_1 \rightarrow gs$	5	3.5853	3.5851	0.74
$(2p_{1/2}^5 3s_{1/2} 3p_{1/2} 3p_{3/2})_1 \rightarrow gs$	6*		3.6107	0.16
$(2p_{1/2}^5 3s_{1/2} 3p_{1/2} 3p_{3/2})_1 \rightarrow gs$	7*		3.6316	0.07
$(2p_{3/2}^5 3s_{1/2} 3p_{3/2} 3p_{3/2})_1 \rightarrow gs$	8*	bl	3.7427	0.21
$(2p_{3/2}^5 3s^2 3d_{5/2})_1 \rightarrow gs$	9	3.7598	3.7592	1.59
$(2p_{3/2}^5 3s_{1/2} 3p_{3/2} 3p_{3/2})_1 \rightarrow gs$	10*	ur	3.7685	0.10
$(2p_{3/2}^5 3s_{1/2} 3p_{3/2} 3p_{3/2})_1 \rightarrow gs$	11*	bl	3.8016	0.06
$3s \rightarrow 2p$ ( $3s, 3p$ spectators)				
$(2p_{1/2}^5 3s^2 3p_{1/2})_0 \rightarrow (2p^6 3s_{1/2} 3p_{1/2})_1$	$\bar{12}$	3.8425	3.8402	0.06
$(2p_{1/2}^5 3s^2 3p_{3/2})_2 \rightarrow (2p^6 3s_{1/2} 3p_{3/2})_2$	$\bar{13}$		3.8609	0.10
$(2p_{1/2}^5 3s^2 3p_{3/2})_1 \rightarrow (2p^6 3s_{1/2} 3p_{3/2})_2$	$\bar{14}$		3.8624	0.09
$(2p_{1/2}^5 3s^2 3p_{1/2})_1 \rightarrow (2p^6 3s_{1/2} 3p_{1/2})_1$	$\bar{15}$		3.8717	0.06
$(2p_{1/2}^5 3s^2 3p_{3/2})_2 \rightarrow (2p^6 3s_{1/2} 3p_{3/2})_1$	$\bar{16}$		3.8895	0.08
$(2p_{1/2}^5 3s^2 3p_{3/2})_0 \rightarrow (2p^6 3s_{1/2} 3p_{3/2})_1$	$\bar{18}$		4.0784	0.06
$(2p_{3/2}^5 3s^2 3p_{3/2})_2 \rightarrow (2p^6 3s_{1/2} 3p_{3/2})_2$	$\bar{19}$		4.0837	0.08
$(2p_{3/2}^5 3s^2 3p_{1/2})_1 \rightarrow (2p^6 3s_{1/2} 3p_{1/2})_0$	$\bar{20}$		4.0920	0.06
$(2p_{3/2}^5 3s^2 3p_{1/2})_2 \rightarrow (2p^6 3s_{1/2} 3p_{1/2})_1$	$\bar{21}$	4.0965	4.0981	0.14
$3s \rightarrow 2p$ ( $3s, 3d$ spectators)				
$(2p_{3/2}^5 3s_{1/2} 3p_{3/2} 3p_{3/2})_1 \rightarrow (2p^6 3s_{1/2} 3d_{5/2})_2$	$\bar{17}$		4.0780	0.07

<sup>a</sup>Lines with wavelength  $\lambda \leq 3.90$  Å are referenced to the line  $w$  of iron; those with  $\lambda \geq 3.90$  Å are referenced to the line  $w$  of argon.



ment and to make accurate wavelength measurements. In particular, we have presented high-resolution measurements of neonlike silver. The dominant features observed are the  $3d \rightarrow 2p$  and  $3s \rightarrow 2p$   $E1$  transitions, as for lower- $Z$  elements. The  $3p \rightarrow 2s$   $E1$  transitions could also be identified, as well as the magnetic quadrupole transition. Further, we have observed the three forbidden electric quadrupole lines which are of interest for x-ray lasers. The measured wavelengths of all but the two shortest transitions agree to within 0.8 mÅ with our *ab initio* calculations from the RAC code.

We have been able to identify firmly the most important sodiumlike, magnesiumlike, and aluminumlike satellites. Again, the  $3d \rightarrow 2p$  transitions are found to be the dominant transitions. The measured wavelengths agree with the computed ones from the RAC code to within approximately 2 mÅ in most cases. No sodiumlike lines resulting from dielectronic recombination are observed. This is consistent with their predicted intensities and the signal-to-noise ratio of the experiment. Instead, the lines that are observed seem excited predominantly via direct excitation from the ground state or via subsequent radiative cascades and inner-shell ionization of the adjacent lower charge state.

The presence of seven different hydrogenlike and heliumlike spectra in the wavelength region investigated has provided us with a number of very reliable reference lines. This set of atomic data has allowed us to determine the wavelengths of the silver lines with high accuracy. It has also enabled us to compare the wavelength calculations for hydrogenlike and heliumlike systems to each other, and a discrepancy of approximately 0.4 mÅ between the Ly- $\alpha$  and the heliumlike  $K\alpha$  lines, which is larger than our experimental uncertainty, has been noted.

Neonlike spectra from tokamak observations are understood more easily than spectra from laser-produced or z-

pinch plasmas. In high-density, highly collisional laser-produced plasmas, for example, collisions between excited states affect their respective populations. This can manifest itself in density-sensitive line ratios<sup>21</sup> or in density-sensitive gain predictions for soft-x-ray lasers;<sup>24</sup> furthermore, the short time scales of laser-produced plasmas may not allow a steady-state ionization balance. The electron and ion densities in tokamaks are many orders of magnitude lower than in the other types of laboratory plasmas. The resulting lack of collisions thus makes low-density plasmas ideal not only for line identifications but also for investigating the excitation mechanisms of neonlike ions. As a first attempt, we have compared the experimental intensities of the neonlike transitions to predictions from a simple collisional excitation and radiative decay model. Although we can note an overall agreement between the data and the predictions, we also note some significant discrepancies. Hence, in order to understand the excitation mechanisms of the neonlike spectra more fully, it will be necessary to investigate the intensity ratios of the neonlike transitions and their satellites in more detail than we have done in this study. In this study we have provided only a survey of the intensity ratios of the neonlike lines to each other. Future studies should include the observation of intensity ratios versus electron temperature and comparisons with detailed theoretical predictions which take into account processes between adjacent ionization stages.

We expect that as the understanding of neonlike systems progresses such systems will become increasingly important for plasma diagnostics. Similar to the well-understood heliumlike spectra, neonlike spectra can be used to measure charge-state abundances and ion and electron temperatures. In present-day tokamaks, such as the PLT or the Tokamak Fusion Test Reactor (TFTR), the electron temperatures are such that most high- $Z$  elements

TABLE IX. Experimental wavelengths and theoretical predictions for  $n=3$  to  $n=2$  transitions in aluminumlike silver. Only selected transitions with  $gf$  larger than 0.10 are listed. ur denotes an unresolved line due to the  $K\alpha$  spectrum of iron, and  $\langle \rangle$  the average wavelength of several unresolved lines.

Transition	Key	$\lambda_{\text{expt}}^a$ (Å)	$\lambda_{\text{theor}}$ (Å)	$gf$
$3p \rightarrow 2s$ ( $3s^2 3p$ spectators)				
$(2s_{1/2} 2p^6 3s^2 3p_{1/2} 3p_{3/2})_{3/2} \rightarrow (2s^2 2p^6 3s^2 3p_{1/2})_{1/2}$	$\alpha$		3.4641	0.32
$(2s_{1/2} 2p^6 3s^2 3p_{1/2} 3p_{3/2})_{1/2} \rightarrow (2s^2 2p^6 3s^2 3p_{1/2})_{1/2}$	$\beta$		3.4684	0.18
$3d \rightarrow 2p$ ( $3s^2 3p$ spectators)				
$(2p_{1/2}^5 3s^2 3p_{1/2} 3d_{3/2})_{3/2} \rightarrow (2p^6 3s^2 3p_{1/2})_{1/2}$	$\gamma$	$\langle 3.6003 \rangle$	3.5977	0.20
$(2p_{1/2}^5 3s^2 3p_{1/2} 3d_{3/2})_{1/2} \rightarrow (2p^6 3s^2 3p_{1/2})_{1/2}$	$\delta$	$\langle 3.6003 \rangle$	3.5993	0.79
$(2p_{1/2}^5 3s^2 3p_{1/2} 3d_{5/2})_{3/2} \rightarrow (2p^6 3s^2 3p_{1/2})_{1/2}$	$\epsilon$		3.6126	0.15
$(2p_{1/2}^5 3s^2 3p_{1/2} 3d_{3/2})_{3/2} \rightarrow (2p^6 3s^2 3p_{1/2})_{1/2}$	$\zeta$	3.6199	3.6198	0.56
$(2p_{1/2}^5 3s^2 3p_{1/2} 3d_{5/2})_{1/2} \rightarrow (2p^6 3s^2 3p_{1/2})_{1/2}$	$\eta$	ur	3.7771	0.55
$(2p_{3/2}^5 3s^2 3p_{1/2} 3d_{5/2})_{1/2} \rightarrow (2p^6 3s^2 3p_{1/2})_{1/2}$	$\theta$	ur	3.7862	0.56
$(2p_{3/2}^5 3s^2 3p_{1/2} 3d_{5/2})_{3/2} \rightarrow (2p^6 3s^2 3p_{1/2})_{1/2}$	$\iota$	3.7918	3.7910	1.35
$(2p_{3/2}^5 3s^2 3p_{1/2} 3d_{3/2})_{3/2} \rightarrow (2p^6 3s^2 3p_{1/2})_{1/2}$	$\kappa$		3.8057	0.12

<sup>a</sup>Lines with wavelength  $\lambda \leq 3.90$  Å are referenced to line  $w$  of iron; those with  $\lambda \geq 3.90$  Å are referenced to line  $w$  of argon.

do not reach the heliumlike charge state. Instead, elements such as silver, molybdenum, or tin are expected to be in the neonlike charge state in the plasma center of these tokamaks. Hence, in order to study, for example, the central diffusion of very high- $Z$  impurities in a tokamak plasma, it is necessary to observe transitions in the neonlike charge state. Similarly, a better understanding of neonlike systems will aid the understanding of the processes involved in astrophysical plasmas or in high-density, laser-produced plasmas.

#### ACKNOWLEDGMENTS

We gratefully acknowledge the help and support of many colleagues, in particular P. Colestock, J. Hosea, and

R. Wilson for their support in making these measurements possible and R. Bell, A. Cavallo, and E. Hinnov for their diagnostic information. We also appreciate discussions with R. Deslattes from the U.S. National Bureau of Standards, with U. Feldman from the Naval Research Laboratory, and with M. Cornille, J. Duban, and M. Loulergue from the Observatoire de Paris. We are grateful for the technical support of J. Gorman, J. Lehner, E. Ruffin, T. Bennett, and the PLT operating crew. This work was supported by U.S. Department of Energy Contracts No. DE-AC02-76-CHO-3073 and No. W-7405-ENG-38. One of the authors (P.B.) was supported by the Fannie and John Hertz Foundation.

- <sup>1</sup>V. A. Abramov, A. B. Berlizov, V. V. Buzankin, A. H. Ver-  
tiporokh, V. A. Vershkov, V. A. Krupin, and G. E. Notkin, in  
*Proceedings of the 8th European Conference on Fusion and  
Plasma Physics, Prague, Czechoslovakia, 1977* (Institute of  
Plasma Physics, Czechoslovak Academy of Sciences, Prague,  
1977), Vol. I, p. 30.
- <sup>2</sup>M. Klapisch, A. Bar Shalom, J. L. Schwob, B. S. Fraenkel, C.  
Breton, C. de Michelis, M. Finkenthal, and M. Mattioli, *Phys.*  
*Lett.* **69A**, 34 (1978).
- <sup>3</sup>S. von Goeler, M. Bitter, S. Cohen, D. Eames, K. W. Hill, D.  
Hills, R. Hulse, G. Lenner, D. Manos, P. Roney, N. Sauthoff,  
S. Sesnic, W. Stodiek, F. Tenney, and J. Timberlake, in  
*Proceedings of the Course on Diagnostics for Fusion Reactor  
Conditions, Varenna, Italy, 1982*, edited by P. E. Scott *et al.*  
(Commission of the European Communities, Brussels, 1983),  
Vol. I, p. 109.
- <sup>4</sup>E. Källne, J. Källne, and R. D. Cowan, *Phys. Rev. A* **27**, 2682  
(1983).
- <sup>5</sup>P. G. Burkhalter, D. J. Nagel, and R. D. Cowan, *Phys. Rev. A*  
**11**, 782 (1975).
- <sup>6</sup>H. Gordon, M. G. Hobby, N. J. Peacock, and R. D. Cowan, *J.*  
*Phys. B* **12**, 881 (1979).
- <sup>7</sup>H. Gordon, M. G. Hobby, and N. J. Peacock, *J. Phys. B* **13**,  
1985 (1980).
- <sup>8</sup>Y. Conturie, B. Yaakobi, U. Feldman, G. A. Doschek, and R.  
D. Cowan, *J. Opt. Soc. Am.* **71**, 1309 (1981).
- <sup>9</sup>P. G. Burkhalter, J. Shiloh, A. Fisher, and R. D. Cowan, *J.*  
*Appl. Phys.* **50**, 4532 (1979).
- <sup>10</sup>P. G. Burkhalter, C. M. Dozier, and D. J. Nagel, *Phys. Rev.*  
*A* **15**, 700 (1977).
- <sup>11</sup>E. V. Aglitsky, E. Ya Golts, Yu A. Levykin, and A. M.  
Livshits, *J. Phys. B* **14**, 1549 (1981).
- <sup>12</sup>J. H. Parkinson, *Astron. Astrophys.* **24**, 215 (1973).
- <sup>13</sup>R. J. Hutcheon, J. P. Pye, and K. D. Evans, *Mon. Not. R.*  
*Astron. Soc.* **175**, 489 (1976).
- <sup>14</sup>D. L. McKenzie, P. B. Landecker, R. M. Broussard, H. R.  
Ruge, R. M. Young, U. Feldman, and G. A. Doschek, *As-*  
*trophys. J.* **241**, 409 (1980).
- <sup>15</sup>K. J. H. Phillips, J. W. Leibacher, C. J. Wolfson, J. H. Parkin-  
son, B. C. Fawcett, B. J. Kent, H. E. Mason, L. W. Acton, J.  
L. Culhane, and A. H. Gabriel, *Astrophys. J.* **256**, 774 (1982).
- <sup>16</sup>D. Eames, Ph.D. thesis, Princeton University, 1980.
- <sup>17</sup>S. A. Cohen *et al.*, *Bull. Am. Phys. Soc.* **28**, 1127 (1983).
- <sup>18</sup>D. Edmondson, S. von Goeler, M. Bitter, S. Cohen, K. Hill,  
N. Sauthoff, S. Sesnic, F. Tenney, and J. Timberlake, *Bull.*  
*Am. Phys. Soc.* **28**, 1128 (1983).
- <sup>19</sup>M. Loulergue and H. Nussbaumer, *Astron. Astrophys.* **24**, 209  
(1973).
- <sup>20</sup>R. Stewart, Ph.D. thesis, University of California, 1985.
- <sup>21</sup>J. Bailey, R. E. Stewart, J. D. Kilkenny, R. S. Walling, T.  
Phillips, R. J. Fortner, and R. W. Lee, *J. Phys. B* (to be pub-  
lished).
- <sup>22</sup>M. Bitter, S. von Goeler, M. Goldman, K. W. Hill, R. Horton,  
W. Roney, N. Sauthoff, and W. Stodiek, in *Temperature, its  
Measurement and Control in Science and Industry*, edited by  
S. F. Schooley (AIP, New York, 1982), Vol. 5, p. 693.
- <sup>23</sup>M. Bitter, K. W. Hill, M. Zarnstorff, S. von Goeler, R. Hulse,  
L. C. Johnson, N. R. Sauthoff, S. Sesnic, and K. M. Young,  
*Phys. Rev. A* **32**, 3011 (1985).
- <sup>24</sup>M. Rosen, P. Hagelstein, D. Matthews, E. Campbell, A. Hazi,  
B. L. Whitten, B. MacGowan, R. E. Turner, R. W. Lee, G.  
Charatis, Gar. E. Busch, C. L. Shepard, and P. D. Rockett,  
*Phys. Rev. Lett.* **54**, 106 (1985).
- <sup>25</sup>D. L. Matthews *et al.*, *Phys. Rev. Lett.* **54**, 110 (1985).
- <sup>26</sup>D. D. Dietrich, G. A. Chandler, R. J. Fortner, C. J. Hailey,  
and R. E. Stewart, *Phys. Rev. Lett.* **54**, 1008 (1985).
- <sup>27</sup>M. Bitter, S. von Goeler, R. Horton, M. Goldman, K. Hill, N.  
R. Sauthoff, and W. Stodiek, *Phys. Rev. Lett.* **42**, 304 (1979).
- <sup>28</sup>K. W. Hill, S. von Goeler, M. Bitter, L. Campbell, R. D.  
Cowan, B. Fraenkel, A. Greenberger, R. Horton, J. Hovey,  
W. Roney, N. R. Sauthoff, and W. Stodiek, *Phys. Rev. A* **19**,  
1770 (1979).
- <sup>29</sup>R. W. G. Wyckoff, *Crystal Structures*, 2nd ed. (Wiley, New  
York, 1963), Vol. I.
- <sup>30</sup>A. H. Gabriel, *Mon. Not. R. Astron. Soc.* **160**, 99 (1972).
- <sup>31</sup>L. A. Vainshtein and U. I. Safronova, *Phys. Scr.* **31**, 519  
(1985).
- <sup>32</sup>P. Mohr, *At. Data Nucl. Data Tables* **29**, 453 (1983).
- <sup>33</sup>A. H. Compton and S. K. Allison, *X-Rays in Theory and Ex-*  
*periment*, 2nd ed. (Van Nostrand, Princeton, 1935), p. 674.
- <sup>34</sup>A. H. Compton and S. K. Allison, *Ref.* **33**, p. 206.
- <sup>35</sup>F. Bely-Dubau, A. H. Gabriel, and S. Volonté, *Mon. Not. R.*  
*Astron. Soc.* **189**, 801 (1979).
- <sup>36</sup>M. Bitter, S. von Goeler, K. W. Hill, R. Horton, D. Johnson,  
W. Roney, N. Sauthoff, E. Silver, and W. Stodiek, *Phys. Rev.*  
*Lett.* **47**, 921 (1981).
- <sup>37</sup>M. Bitter, S. von Goeler, S. Cohen, K. W. Hill, S. Sesnic, F.  
Tenney, J. Timberlake, U. I. Safronova, L. A. Vainshtein, J.  
Dubau, M. Loulergue, F. Bely-Dubau, and L. Steenman-  
Clark, *Phys. Rev. A* **29**, 661 (1984).
- <sup>38</sup>U. I. Safronova, *Phys. Scr.* **23**, 241 (1981).
- <sup>39</sup>J. P. Briand, M. Tavernier, P. Indelicato, R. Marrus, and H.

- Gould, Phys. Rev. Lett. **50**, 832 (1983).
- <sup>40</sup>J. P. Briand, J. P. Mossé, P. Indelicato, P. Chevallier, D. Girard-Vernhet, and A. Chetioui, Phys. Rev. A **28**, 1413 (1983).
- <sup>41</sup>TFR Group, M. Cornille, J. Dubau, and M. Loulergue, Phys. Rev. A **32**, 3000 (1985).
- <sup>42</sup>E. S. Marmar, J. L. Cecchi, and S. A. Cohen, Rev. Sci. Instrum. **46**, 1149 (1975).
- <sup>43</sup>S. Cohen *et al.*, J. Vac. Sci. Technol. **20**, 1226 (1982).
- <sup>44</sup>M. Loulergue and H. Nussbaumer, Astron. Astrophys. **45**, 125 (1975).
- <sup>45</sup>P. L. Hagelstein, Plasma Phys. **25**, 1345 (1983).
- <sup>46</sup>I. P. Grant, B. J. McKenzie, P. H. Norrington, D. F. Mayers, and N. C. Pyper, Comput. Phys. Commun. **21**, 207 (1980).
- <sup>47</sup>M. H. Chen, Phys. Rev. A **31**, 1449 (1985).
- <sup>48</sup>P. L. Hagelstein and R. K. Jung, At. Data Nucl. Data Tables (to be published).
- <sup>49</sup>B. W. Smith, J. C. Raymond, J. B. Mann, and R. D. Cowan, Astrophys. J. **298**, 898 (1985).
- <sup>50</sup>B. L. Whitten, A. U. Hazi, M. H. Chen, and P. L. Hagelstein, Phys. Rev. A **33**, 2171 (1986).